REACTIVITY INITIATED ACCIDENT TEST SERIES
RIA SCOPING TEST
EXPERIMENT PREDICTIONS

R.S. SEMKEN   A.M. EATON

R.H. SMITH   S.C. RESCH

June 1978

EXPORT REVIEW COMPLETED
NO LICENSE REQUIRED

EC 65014

EG&G Idaho, Inc.

IDAHO NATIONAL ENGINEERING LABORATORY

DEPARTMENT OF ENERGY

IDAHO OPERATIONS OFFICE UNDER CONTRACT EY-76-C-07-1570

PDF Available
Common

REACTIVITY INITIATED ACCIDENT TEST SERIES
RIA SCOPING TEST
EXPERIMENT PREDICTIONS

R.S. SEMKEN   A.M. EATON

R.H. SMITH   S.C. RESCH

June 1978

EG&G Idaho, Inc.

IDAHO NATIONAL ENGINEERING LABORATORY

DEPARTMENT OF ENERGY

REACTIVITY INITIATED ACCIDENT TEST SERIES SCOPING TEST

EXPERIMENT PREDICTIONS

R. S. Semken
A. M. Eaton
R. H. Smith
S. C. Resch

Approved:

Z. R. Martinson / R.SS.
Z. R. Martinson, Project Leader RIA Tests
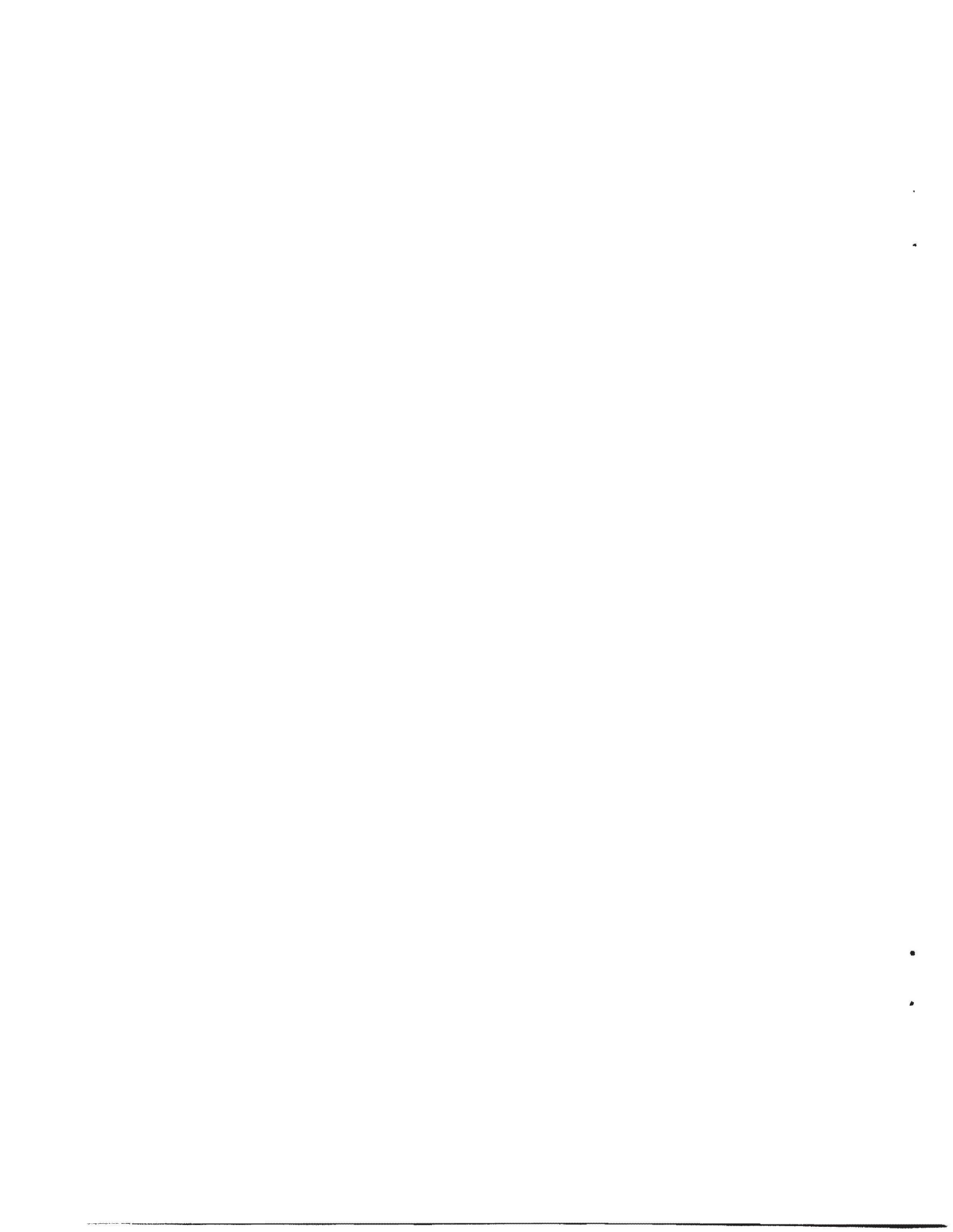
A.S. Mehner/RKM
A. S. Mehner, Supervisor
PCM, RIA, IE, and Gap Conductance Tests Section

R.K. McCardell
R. K. McCardell, Acting Manager
Experiment Specification and Analysis Branch

P.P. Irhu J....
P. E. MacDonald, Manager
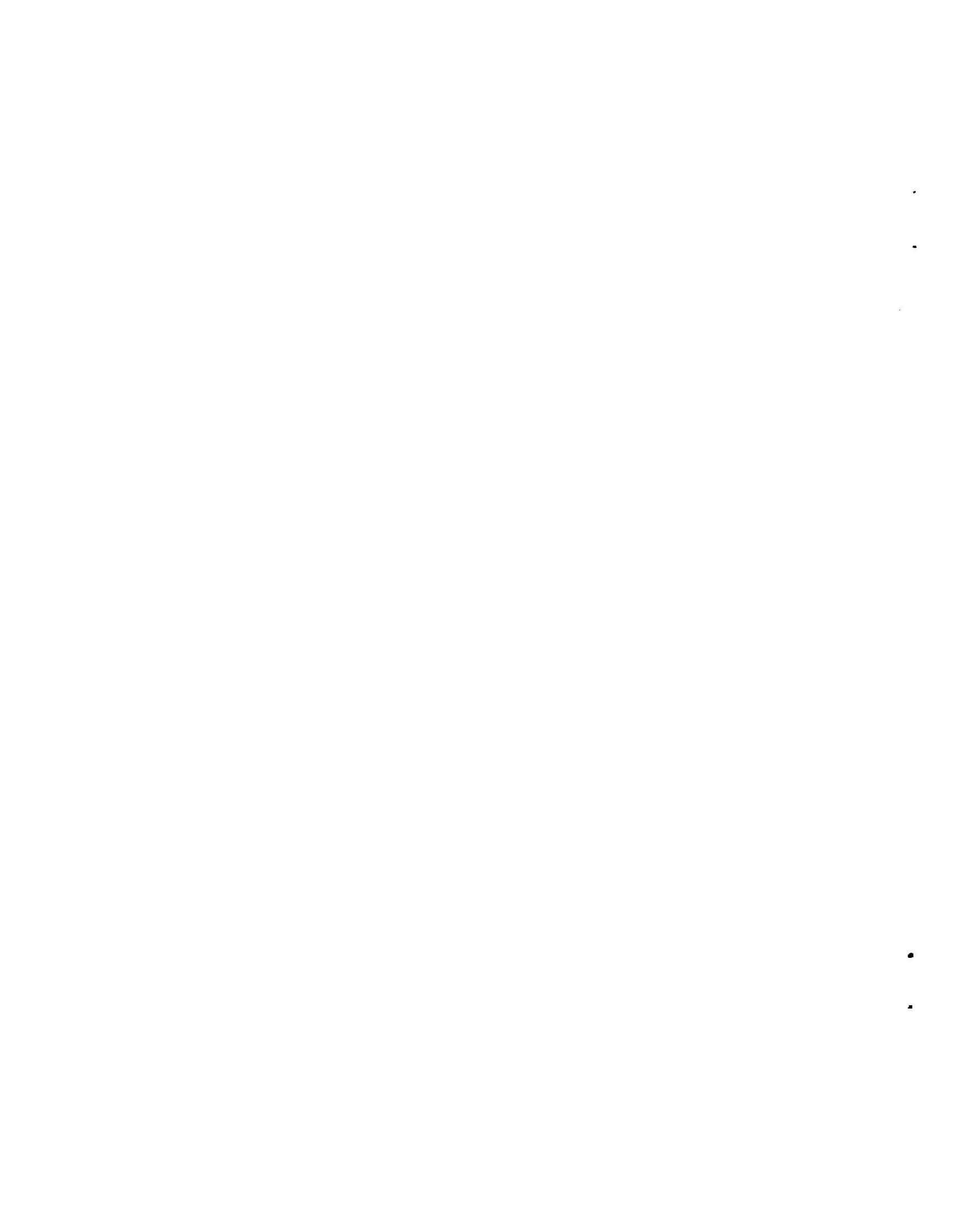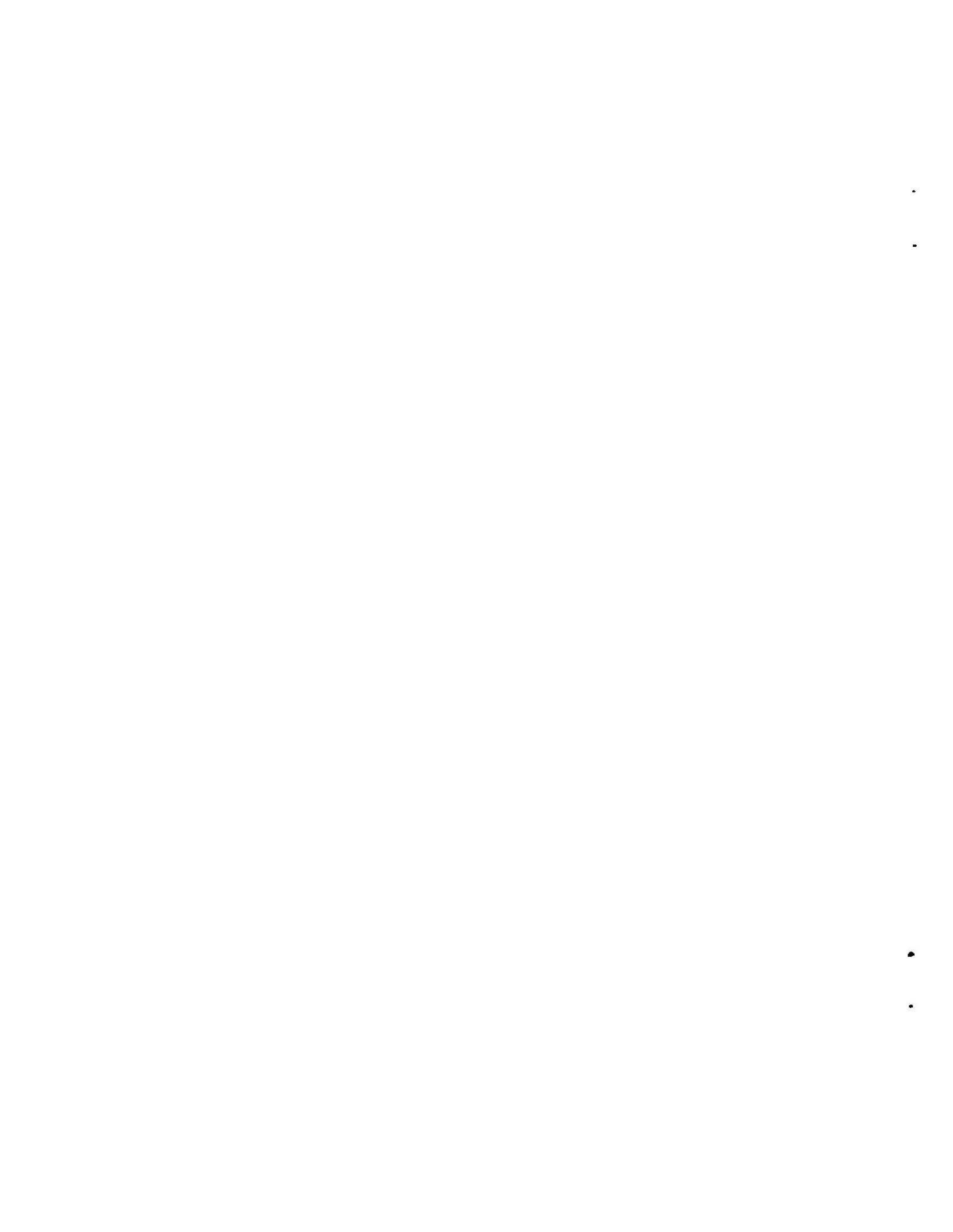Thermal Fuels Behavior Division

CONTENTS

FIGURES

TABLES

SUMMARY

The Reactivity Initiated Accident (RIA) test series to be conducted in the Power Burst Facility (PBF) has been designed to determine fuel failure thresholds, modes, and consequences as a function of energy deposition, irradiation history, and fuel design. The RIA Scoping Test will be comprised of five single unirradiated rod sub-tests. The first rod will be subjected to a series of transient power bursts of increasing energy release to determine the energy deposition at cladding failure. The second and third rods will be subjected to energy depositions near that which caused failure of the first rod, to further define the failure threshold. Rods four and five will be subjected to large radially averaged energy depositions, 1990 and 2510 J/g respectively, to investigate facility safety concerns.

Several analyses were performed to predict test fuel rod and system behavior during the five RIA Scoping Test phases. A reactor physics analysis was performed to obtain the relationship between test fuel rod and reactor core energy during a power transient. The calculations were made with the RAFFLE computer code. The thermal-hydraulic behavior of the test rod coolant was investigated for pellet surface energy depositions of 900, 1125, and 1350 J/g for the first three phases of the Scoping Test. The RELAP4 computer code was used for these thermal-hydraulic analyses. The results of the RELAP4 calculations provided input to the FRAP-T4 computer code for three fuel rod behavior analyses at pellet surface energy depositions of 815, 1020, and 1225 J/g. A cladding embrittlement analysis, using the results of the FRAP-T4 calculations as input, was made to investigate the cladding oxidation mode of rod failure for the lower energy phases. BUILD5 was the analytical tool used in this investigation. Finally, the pressure pulses generated as a result of failure of the test fuel rods in the final two high energy test phases were calculated using the SPIRT computer code.

In previous reactivity initiated accident tests performed in the SPERT, TREAT, and NSRR facilities a pellet surface energy deposition of

1

12.350 x 10^3 J/cm^3 was identified as the failure threshold for unirradiated fuel rods with the ambient test conditions of 300 K, 0.1 MPa, and no forced flow. This volumetric energy deposition is equivalent to a pellet surface energy deposition of 1190 J/g (284 cal/g) when the RIA-ST fuel pellet density of 10.365 g/cm^3 is considered. For no-flow conditions, it was further observed that the presence of a flow shroud caused a reduction of up to 10% in the failure threshold. The modes of failure seen in the previous tests were cladding embrittlement and low pressure rupture as the zircaloy melting temperature was approached. In general, the rod failures occurred only when a peak cladding temperature of 2073 K or above was reached.

Based on the analyses, it is predicted that the test fuel rod energy deposition failure threshold will be 1035 J/g (247 cal/g) at the pellet surface for the fuel rods used in the initial three phases of the RIA Scoping Test. The initial coolant conditions for these cases are equivalent to a fuel enthalpy of 69 J/g (16.5 cal/g) at the fuel surface over ambient conditions. When the difference in initial coolant conditions is considered, the total fuel enthalpy increase leading to cladding failure observed in the previous RIA tests is equivalent to 1122 J/g (268 cal/g) at the fuel pellet surface. The difference between the predicted failure threshold value and that observed in previous tests (87 J/g) is believed to be a combined result of the presence of a flow shroud and uncertainies in the computer codes used to make the predictions. The mode of failure according to the analyses will be rupture due to high temperature cladding weakening. The consequences of these failures are predicted to be minimal. The mode of failure for the high energy phases of the Scoping Test will be cladding rupture due to internal rod pressurization from UO$_2$ vaporization. The high energy rod failures were predicted by the SPIRT code to result in source pressure pulses of 24.1 and 24.8 MPa for the 1990 and 2510 J/g energy depositions, respectively. Pressure doubling will occur in each case with a rise time of 7 ms resulting in maximum pressures of 31.7 and 34.5 MPa, respectively.

1. INTRODUCTION

The Reactivity Initiated Accident Scoping Test (RIA-ST) will investigate the consequences of fuel rod failure during RIA testing in the Power Burst Facility (PBF) at the Idaho National Engineering Laboratory. The test will consist of five subtest phases, each phase beginning with a new single fuel rod. The first three phases, designated RIA-ST-1, RIA-ST-2, and RIA-ST-3, are designed to (a) provide data on the energy deposition threshold beyond which fuel rod failure occurs and (b) develop calorimetric techniques of determining rod power during a transient. The final phases, RIA-ST-4 and RIA-ST-5, are not programmatic tests but were designed to identify the magnitude of pressure pulses expected as a result of large energy depositions[a].

This Experiment Predictions report addresses three aspects of the RIA Scoping Test. First, the fuel rod energy as a function of PBF reactor core energy for the fuel rod configuration used in the first three test phases is predicted based on reactor physics code calculations. Second, the failure energy deposition threshold and the mode of failure are predicted for the first three test phases based on the results of thermal-hydraulic and fuel rod behavior code analyses, cladding embrittlement analysis, and the experimental baseline data obtained from RIA tests conducted in the SPERT, TREAT, and NSRR facilities. Finally, the mode of failure for the two high energy phases, RIA-ST-4 and RIA-ST-5, and the resulting pressure pulses are predicted based on additional fuel rod behavior analysis and SPIRT[b] computer code analyses.

---

[a] PBF operator or system errors could produce radially averaged test rod energy depositions as high as 2510 J/g while performing a planned 1255 J/g four-rod RIA test.

[b] SPIRT: Stress-strain from Pressures Instigated by Reactor Transients, Configuration Control Number P031101.

Section 2 of this report briefly describes the test design and planned conduct for the RIA Scoping Test. The respective analyses performed for the experiment predictions are described in Section 3. Section 4 describes the relevant results of the previous RIA tests performed in the SPERT, TREAT, and NSRR facilities, and in Section 5 the conclusions are presented.

2. TEST DESIGN AND PLANNED CONDUCT

This section of the report contains a brief description of the design and an outline of the conduct for the RIA Scoping Test. A more detailed account can be found in the RIA-ST Experiment Operating Specification[1].

2.1 Test Design

The RIA Scoping Test is comprised of five separate, single-rod test phases. The rod for each phase will be positioned in a separate flow shroud in the center of the PBF in-pile tube (IPT). The design of the fuel rods, test assembly, and instrumentation associated with each component are described in the following paragraphs.

The five fuel rods for the RIA Scoping Test phases are designated as 800-1, 800-2, 800-3, 800-4, and 800-5, respectively. The nominal design characteristics of these rods are given in Table I. The fuel rods were fabricated from unirradiated cladding and fresh fuel pellets. The fuel pellets for Rods 800-1, 800-2, and 800-3 were ground down to fit in available cladding.

Individual zircaloy-4 flow shrouds, having a nominal inner diameter of 16.30 mm and an outer diameter of 22.6 mm, surround each rod. Fuel particle catch screens are installed at the inlet and outlet of the flow shroud for Rods 800-4 and 800-5 only.

The PBF single rod test train assembly will be used for the RIA Scoping Test. In the test assembly, the fuel rod is held rigidly at the top, with the rod free to expand axially downward.

2.2 Instrumentation

The instrumentation in the test is provided for pressure pulse measurement, calorimetric measurement of the test rod power, and evaluation

TABLE I

RIA SCOPING TEST FUEL ROD DESIGN CHARACTERISTICS

Characteristic	Rods 800-1, 2, 3	Rods 800-4, 5
Fuel		
Material	UO_2	UO_2
Pellet OD (mm)	8.23 + 0.0127	9.3 + 0.0127
Pellet length (mm)	15.2	15.49
Pellet enrichment (%)	5.8	20
Density (% TD)	94.5	93
Fuel stack length (m)	0.914	0.914
End configuration	Dished	Dished
Burnup	0	0
Cladding		
Material	Zr-4	Zr-4
Tube OD (mm)	9.70	10.73
Tube wall thickness (mm)	0.64	0.61
Fuel Rod		
Overall length (m)	1.0	1.0
Filler Gas	Helium	Helium
Initial gas pressure (MPa)	0.103	2.6

of instrumentation to be used in future RIA tests. No instrumentation will be installed on the test fuel rods. A linear variable differential transformer (LVDT), mounted on the test train, will measure cladding elongation for phases RIA-ST-1, RIA-ST-2, and RIA-ST-3.

The test assembly instrumentation consists of the following:

(1) Three coolant pressure transducers, two located above the flow shroud outlet, and one located below the fuel rod to measure the transient pressure response and normal system pressure.

(2) Two turbine flowmeters, mounted in series at the inlet of the flow shroud, to measure the coolant flow through the shroud.

(3) Four thermocouples, two mounted on the shroud inlet and two at the outlet, to measure the coolant temperature at inlet and outlet.

(4) Two differential thermocouples mounted on the test train to measure the coolant temperature rise across the flow shroud.

(5) Three cobalt self-powered neutron detectors (SPND) located in one vertical column at 0.229, 0.457 and 0.686 m above the bottom of the test fuel rod.

(6) One flux wire mounted on the outer surface of the flow shroud for each phase of the test.

(7) Five pressure transducers located in the flow bypass region for radiation sensitivity evaluation.

(8) One linear variable differential transformer (LVDT) mounted at the bottom of the fuel rod to measure changes in axial length of the fuel rod. The LVDT will be removed for RIA-ST-4 and RIA-ST-5 to allow a more precise measurement of the expected pressure pulse.

7

(9) Another LVDT, with its core locked in position, located below
     the fuel rod for radiation sensitivity evaluation.

2.3 Test Conduct

The five test phases of the RIA Scoping Test will be designated as
RIA-ST-1 through RIA-ST-5. Table II summarizes the various activities
associated with the five test phases. Details of the test conduct are
discussed in the following paragraphs. Nuclear operation will start
after loop heatup and terminate immediately after each transient.

There will be a power calibration for test phases RIA-ST-1, RIA-ST-4,
and RIA-ST-5. The objective of the power calibrations will be to inter-
calibrate the thermal-hydraulically determined fuel power with reactor
power and the self-powered neutron detector (SPND) output. The on-line
power calibration will be accomplished by measuring the coolant pres-
sure, coolant inlet temperature, coolant temperature rise, and coolant
flow. An axial peak-to-average neutron flux ratio of 1.36 will be used
for preliminary calculations. The coolant conditions during the power
calibration will be 538 K, 6.45 MPa, and 760 cm^3/s at the test train
inlet. The fuel rod peak power will not exceed 52 kW/m during the power
calibration.

RIA-ST-1 will include a fuel rod preconditioning phase to build up
the fission product inventory of the fuel rod and to cause fuel pellet
cracking. The preconditioning will be performed at a fuel rod peak
power of 52 kW/m. The coolant conditions will be 538 K, 6.45 MPa, and
760 cm^3/s at the test train inlet.

The test train inlet coolant conditions for each power transient
will be 538 K, 6.45 MPa, and 85 cm^3/s. The reactor transient period
for each phase of the test will be chosen on the basis of the RIA
Scoping Test power calibration results and PBF lead rod test data.

8

TABLE II

RIA SCOPING TEST PLAN[a]

RIA-ST-1	RIA-ST-2	RIA-ST-3	RIA-ST-4	RIA-ST-5
Heat Up	Heat Up	Heat Up	Heat Up	Heat Up
Power calibration	Single transient at failure energy.	Single transient at ST-1 failure energy minus 210 J/g if rod fails in ST-2; single transient at ST-1 failure energy plus 210 J/g if rod does not fail in ST-2.	Power calibration	Power calibration
Shutdown			Shutdown	Shutdown
Core flux wire change	Cooldown		Core flux wire change single transient at 1990 J/g	Core flux wire change single transient at 2510 J/g
Fuel rod preconditioning				
Shutdown			Cooldown	Cooldown
Core flux wire change		Cooldown		
835 J/g (900 J/g pellet surface) transient				
Shutdown				
Core flux wire change				
1045 J/g (1125 J/g pellet surface) transient				
Shutdown				
Core flux wire change				
1140 J/g (1240 J/g pellet surface) transient				
Shutdown				
Core flux wire change				
1255 J/g (1350 J/g pellet surface) transient				
Continued until rod failure				
Cooldown				

[a] Unless otherwise noted, all energy deposition values are radially averaged energies deposited at the axial power peak elevation.

3. TEST PREDICTION ANALYSIS

A discussion of the analyses performed for the test predictions
and a presentation of the results are contained in this section.
The reactor physics analysis is discussed first, followed by the
thermal-hydraulic analyses, fuel rod behavior analyses, cladding
embrittlement analysis, and finally the pressure pulse analyses.

3.1 Reactor Physics Analysis

The reactor physics calculations were done to predict fuel rod
energy as a function of PBF reactor core energy for Rods 800-1, 800-2,
and 800-3. These are the 9.70 mm OD fuel rods to be used in the three
initial test phases.

The reactor physics calculations[2] were performed by the EG&G
Reactor Physics Engineering Branch using the SCAMP Sn-transport theory
code[a,3]. The amount of energy deposited into the test rod and PBF
driver core was calculated using the factors of 178.2 MeV/fission for
the test fuel and 186.4 MeV/fission for the driver core. These values
include no contribution from delayed gammas or betas, since more than
99% of the energy deposition due to these components does not occur
until after the completion of the transient.

The radial power profile calculated for the 9.70 mm OD fuel rods
by the SCAMP code is shown in Table III. The radial peak-to-average
power ratio is 1.076 with the peak located at the pellet surface.

---

[a] SCAMP, Configuration Control Number H000029IB. ENDF/B-II, -III,
-IV Library, Configuration Control Number H001701B.

TABLE III

ENERGY DEPOSITION IN 9.70 mm OD TEST FUEL ROD

Region	Outer Radius (mm)	Axial Average Energy[a]	Axial Peak Energy[a]
1	1.84	2.897	3.940
2	2.60	2.977	4.049
3	3.19	3.065	4.168
4	3.68	3.169	4.310
5	4.12	3.320	4.515
Average		3.086	4.197

[a] Joules absorbed per gram of UO_2 in the test rod for each megawatt-second of energy deposited in the PBF driver core. The axial peak was assumed to be 1.36 times the axial average.

3.2 Thermal-Hydraulic Analyses

Three thermal-hydraulic analyses were made with RELAP4[a,4] to provide data on the IPT coolant behavior during three RIA power transients. These data were used as coolant boundary conditions for three fuel rod behavior analyses. A RELAP4 transient model of the PBF in-pile tube was developed and is described in Appendix A.

The three analyses considered axial power peak energy depositions of 900, 1125, and 1350 J/g (215, 270, and 325 cal/g) at the pellet surface of the fuel of the 9.70 mm OD fuel rods. The normalized power and energy histories used for each analysis are shown in Figure 1. These curves are based on a PBF reactor period power transient of 3.5 ms. Scaling factors were applied to the normalized power and energy histories to achieve the desired energy depositions in the RELAP4 calculations. The calculations were run for 29 s following the initiation of each power transient at 1.0 s.

The initial test train inlet coolant conditions assumed in the analyses were 538 K, 6.45 MPa, and 495 kg/m^2·s ($\sim$85 cm^3/s). The magnitude of the inlet pressure necessitated the use of an interpolation between the Barnett and modified Barnett critical heat flux (CHF) correlations. The Groeneveld 5.7 film boiling correlation was used for post-CHF calculations.

The results of the RELAP4 analysis describing the coolant behavior for the 1350 J/g energy deposition are illustrated by Figures 2 through 5. Since the results of the 900 and 1125 J/g deposition calculations were similar to those for the 1350 J/g case, they are discussed only briefly.

Figures 2 and 3 describe the coolant flow shroud inlet and outlet mass flow rates, respectively, as a function of time. At approximately

---

[a] RELAP/MOD5, Configuration Control Number H00330IB.
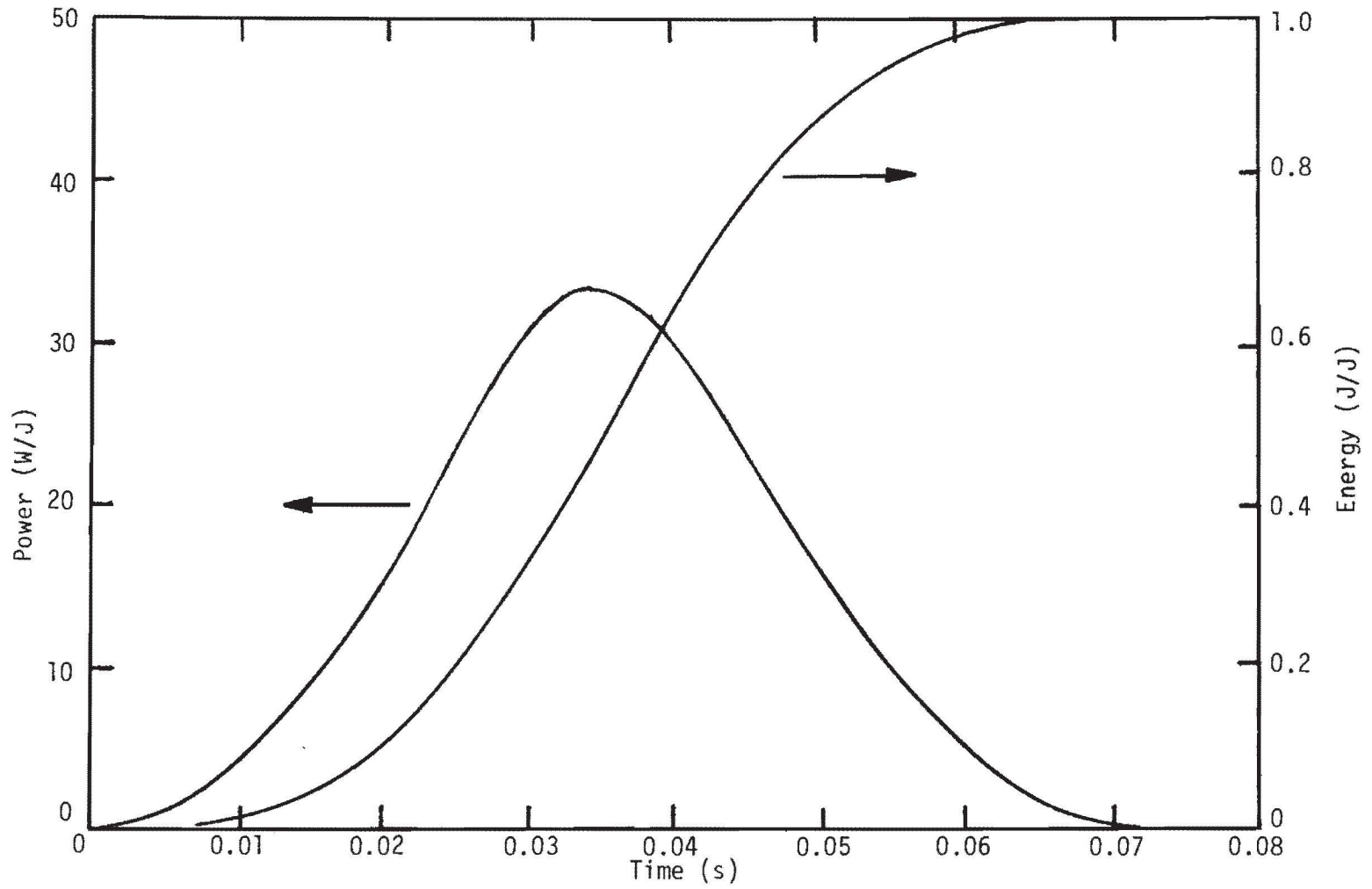
Fig. 1   PBF 3.5 ms period power and energy histories (normalized to total energy produced).

13
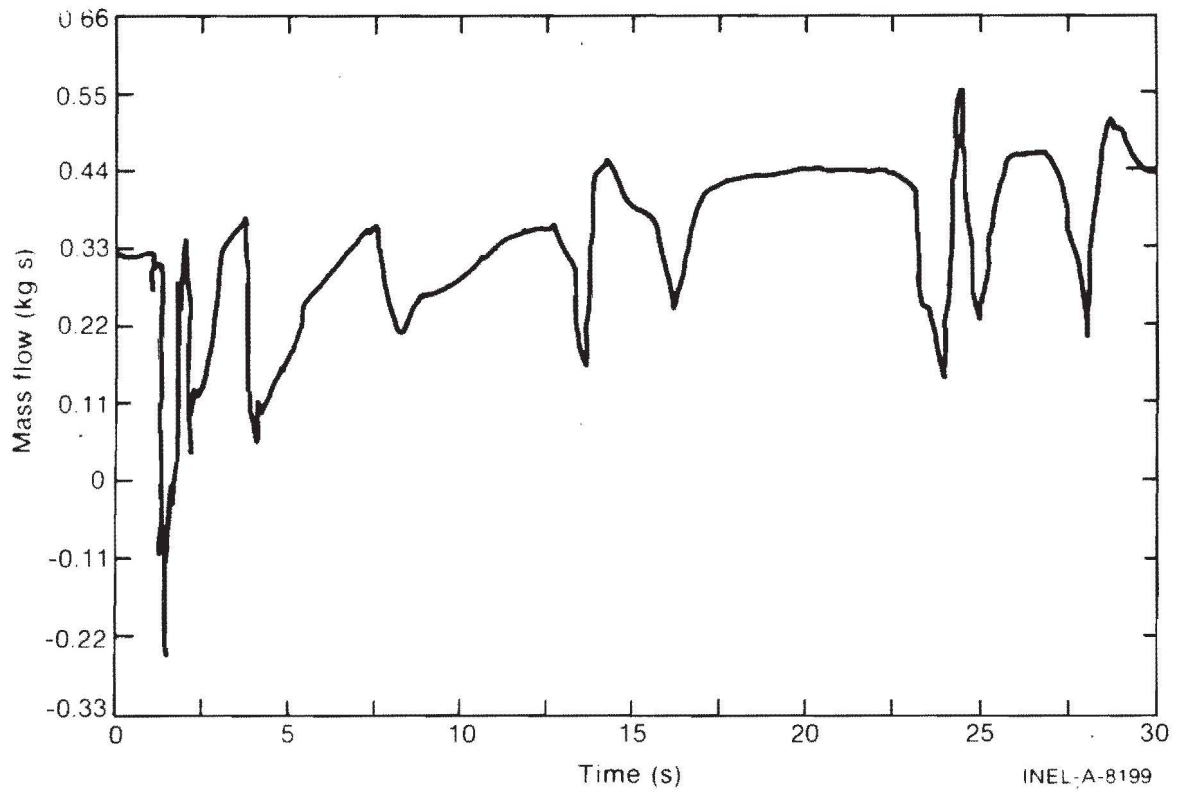
Fig. 2 Inlet coolant mass flowrate history for a 1350 J/g pellet surface energy deposition.
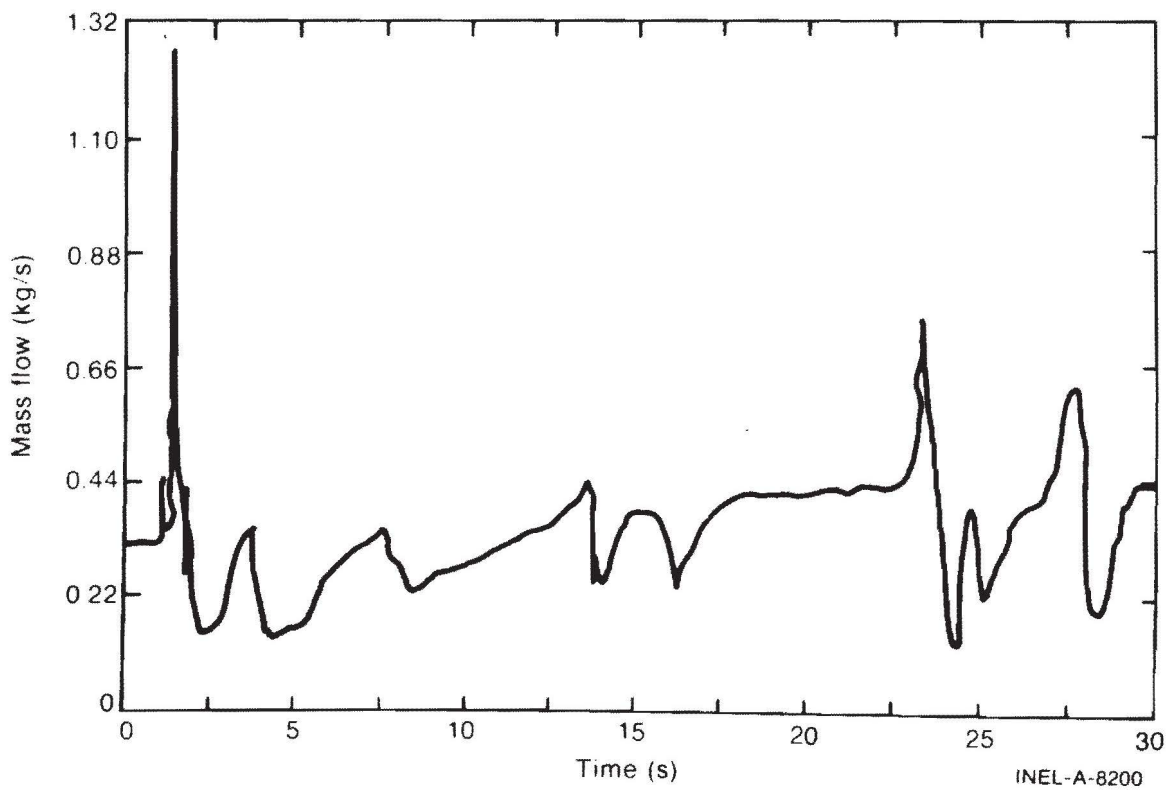
Fig. 3 Outlet coolant mass flowrate history for a 1350 J/g pellet surface energy deposition.

14

0.5 s after the transient initiation, a flow reversal at the coolant inlet with a peak mass flowrate of -0.25 kg/s and a flow surge at the coolant outlet with a peak magnitude of 1.27 kg/s are indicated. This is due to initial coolant vaporization and subsequent rapid flow shroud voiding. Positive flow at the coolant inlet is reestablished a short time thereafter. After the resumption of positive flow, Figures 2 and 3 indicate that the coolant inlet and outlet flows oscillate. These oscillations are believed to be due to thermal changes occurring in RELAP4 at this stage of the analysis, in particular, changes in heat transfer mode and coolant quality.

Figure 4 illustrates the coolant quality as a function of time at the axial hot spot and coolant outlet locations. Peak qualities of 16 and 36% are indicated for the two locations, respectively. The peaks occur about 1.5 s after transient initiation. The sporadic increases in quality, which are indicated by Figure 4 during the decline in quality, occur in response to heat transfer mode changes within the RELAP4 calculational mechanism. Coolant quality at the hot spot reached zero after about 25 s.

Figure 5 illustrates the coolant temperature at the axial hot spot as a function of time. The temperature is shown to reach saturation (552.5 K) almost immediately. At about 22 s the brief drop in temperature indicates a temporary resumption of single phase flow and then, because of quality increases upstream, a jump back to two phase flow with an accompanying increase in quality (Figure 4).

The results of the RELAP4 calculations for a 900 J/g energy deposition also indicated a flow reversal at the shroud inlet and a flow surge at the outlet. The flow reversal and surge were shown to peak at -0.025 kg/s and 0.18 kg/s, respectively. Positive flow was resumed at the inlet within 1.0 s. Coolant quality at the axial hot spot peaked at about 9% approximately 2 s after transient initiation. It reached zero at about 14 s. Coolant quality at the shroud outlet peaked at 13% almost 8 s after the transient. It returned to zero at about 24 s. Coolant temperature at the axial hot spot increased to saturation within 0.3 s of

15
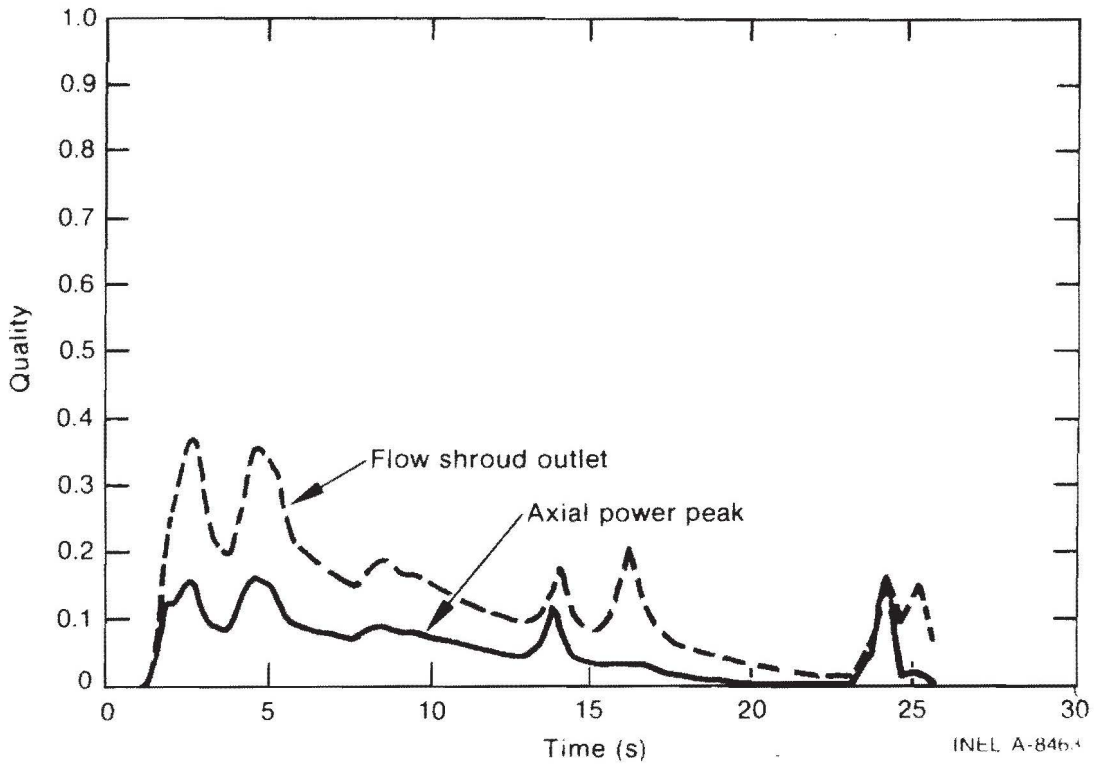
Fig. 4 Coolant qualities at the axial power peak and flow shroud outlet for a 1350 J/g pellet surface energy deposition.
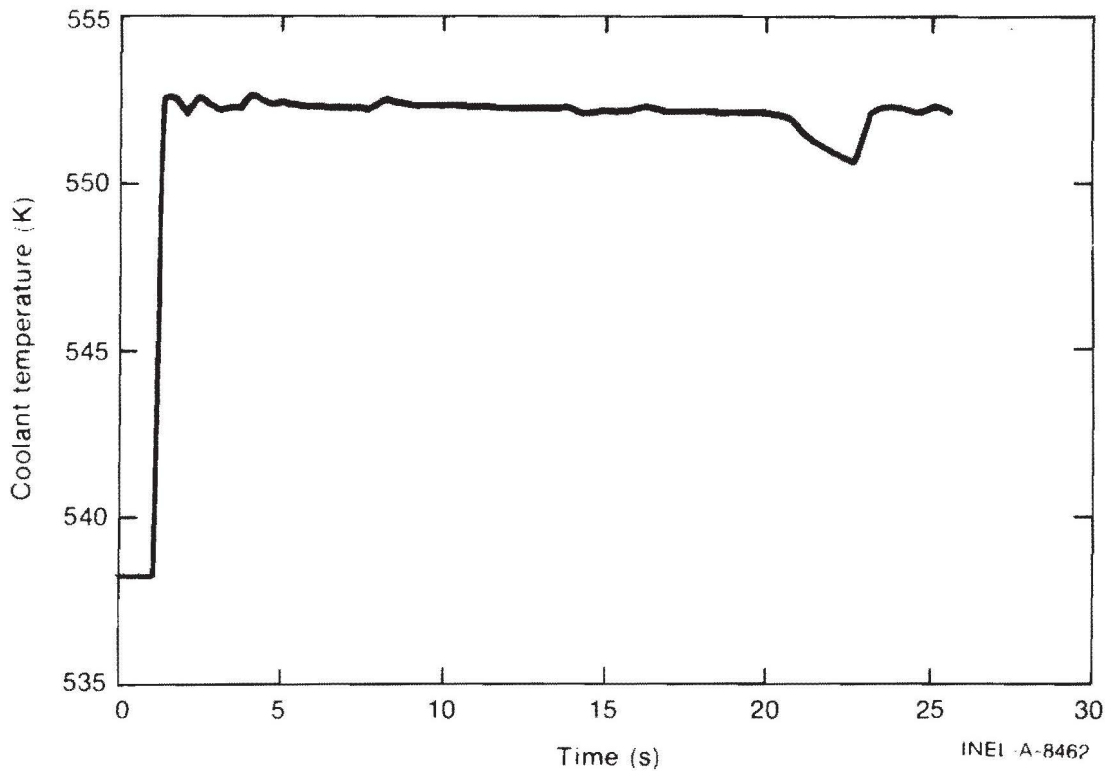
Fig. 5 Coolant temperature history at the axial power peak location for a 1350 J/g pellet surface energy deposition.

16

transient initiation and remained near this temperature for the next 21.5 s after which it began decreasing to the initial coolant temperature.

The results of the 1125 J/g deposition calculations indicated a flow reversal and flow surge peaking at -0.045 kg/s and 0.20 kg/s. Positive flow conditions were reestablished within 1 s. Coolant quality was shown to reach 15% at the hot spot almost 4 s after transient initiation and to decline to zero at 17.5 s. After a 1 s delay, the quality at the flow shroud outlet ramped up to a peak value of 22%, reaching it 4.5 s after transient initiation. It then declined to zero within 27 s from the time of transient initiation. Coolant temperature reached saturation within 0.2 s and remained close to saturation for almost 25 s. The temperature then began falling rapidly back to the initial condition temperature.

3.3 Fuel Rod Behavior Analyses

The analytical model used for the fuel rod thermal and mechanical behavior analyses was the Fuel Rod Analysis Program - Transient Version 4 (FRAP-T4) computer code [a,5]. FRAP-T4 is a general purpose code designed to analyze the behavior of nuclear fuel rods subjected to transient conditions. The behavior of a rod is predicted by using an iterative solution technique that combines and couples the effects of thermal, mechanical, and material properties. FRAP-T4 prediction analyses were made to provide data on the energy deposition failure threshold for the following cases:

(1) a 9.70 mm OD fuel rod with a pellet surface, axial peak energy deposition of 815 J/g (195 cal/g),

(2) a 9.70 mm OD fuel rod with a pellet surface, axial peak energy deposition of 950 J/g (245 cal/g),

---

[a] FRAP-T4, Version 9/16, Configuration Control Number H003251B

(3)   a 9.70 mm OD fuel rod with a pellet surface, axial peak
       energy deposition of 1225 J/g (295 cal/g), and

(4)   a 10.73 mm OD fuel rod with a radially averaged, axial peak
       energy deposition of 2510 J/g (600 cal/g).

The coolant conditions (pressure, temperature, enthalpy, and mass
flux) calculated by the three RELAP4 models discussed in Section 3.2 were
used as the input coolant boundary conditions for the three 9.70 mm OD
fuel rod behavior calculations. The small differences in the energy
depositions between the RELAP4 and FRAP-T4 calculations will not create
significant errors. The coolant conditions for the 10.73 mm OD fuel
rod calculations were idealized by inputting to the coolant an estimate
of the axially averaged enthalpy resulting from the 2510 J/g power
transient[a].

The FRAP-T4 model used 18 equi-spaced axial nodes for calculational
purposes with heat transfer correlations identical to those used in the
RELAP4 analyses. The same power-time history that was used in the RELAP4
analyses (Figure 1) was also used for these FRAP-T4 analyses. Calcula-
tions for cases 1, 2, and 3 were continued for more than 25 s in each
case after the start of the power transient. At this time the entire
fuel rod length had quenched in each case. For case 4, the calculations
were discontinued after 1 s because rod failure was indicated. A summary
of the FRAP-T4 input for the four cases is given in Appendix B.

3.3.1   FRAP-T4 Calculations for a Pellet Surface Energy Deposition
of 815 J/g. The results of the FRAP-T4 calculations for a pellet sur-
face energy deposition of 815 J/g are illustrated by Figures 6 through 9.
For this case, the power transient was started at 1.0 s, and the calcu-
lations were continued for 29 s.

---

[a] This idealization is possible because, due to the extremely rapid
    rod failure, there is little time for the rod behavior to be
    influenced by coolant conditions.

18

Fig. 6   Fuel rod temperature histories at the axial power
peak location for an 815 J/g pellet surface deposition.

Fig. 7 Axial fuel centerline, fuel surface, and cladding
surface temperature profiles at the time of the maximum
cladding surface temperature for an 815 J/g pellet surface.

19

Fig. 8 Fuel rod gap width history at the axial power peak
location for an 815 J/g pellet surface energy deposition.

Fig. 9 Fuel stack and cladding axial elongation histories
for an 815 J/g pellet surface energy deposition.

20

Figure 6 illustrates the fuel centerline, fuel surface, and cladding surface temperature histories at the axial power peak elevation of the fuel rod. Almost immediately following the transient, the three temperatures reach their maximums. The maximum fuel centerline temperature is 2440 K. The maximum pellet surface and cladding surface temperatures are 1655 and 1615 K, respectively. Neither the fuel nor the cladding temperatures indicate melting at their respective radial locations. In fact, for this energy deposition, fuel or cladding melting was not indicated anywhere in the fuel rod. All three temperatures of Figure 6 begin ramping down after peaking. At about 14.5 s after transient initiation the pellet and cladding surface temperatures drop sharply, indicating quenching (collapse of film boiling) at the axial power peak elevation. The fuel rod is completely quenched, according to FRAP-T4 at about 15.2 s after transient initiation.

Figure 7 illustrates the FRAP-T4 calculated axial fuel centerline, fuel surface, and cladding surface temperature profiles for the 815 J/g energy deposition. The profiles represent a time of 1.86 s after initiation of the transient when the cladding surface temperature is at a maximum. The cladding and pellet surface profiles indicate which axial nodes are in film boiling at this time (the higher temperatures). FRAP-T4 predicted that 72% of the fuel stack length will enter film boiling immediately after transient initiation.

Gap width at the axial power peak elevation, illustrated in Figure 8, drops immediately to zero from a pre-transient width of 0.092 mm and remains closed for about 16 s. The gap then reopens, increasing first to 0.010 mm. This gap reopening corresponds to the collapse of film boiling at the axial power peak location (Figure 6). After the initial jump, the gap continues to widen, asymptotically approaching 0.025 mm.

Figure 9 illustrates the axial elongation of the fuel stack and cladding as calculated by FRAP-T4. Both curves peak shortly after initiation of the transient. The magnitudes of the peaks are 20.2 mm for the fuel stack and 4.2 mm for the cladding, corresponding to changes

of 18.5 and 3.4 mm from the pre-transient lengths. Shortly before
reaching the maximum fuel stack and cladding elongations and continu-
ously thereafter to about 17 s, the fuel-cladding gap is closed, and as
a result, FRAP-T4 assumes that cladding expansion (contraction) paral-
lels fuel stack expansion (contraction). This assumption results in the
negative cladding elongation, or contraction, seen in Figure 9. At
about 17 s, when the gap opens, the cladding springs back a little
leaving 8.3 mm permanent shrinkage of the cladding length. The ideali-
zation by FRAP-T4 of no slippage between fuel and cladding is believed
to be incorrect in this case. Instead of the large contraction of the
cladding's axial length indicated, fuel pellet separation is expected.

3.3.2 FRAP-T4 Calculations for a Pellet Surface Energy Deposition
of 1020 J/g. The results of the FRAP-T4 analysis for a pellet surface
energy deposition of 1020 J/g are illustrated by Figures 10 through 13.
For this case, the power transient was initiated at 1.0 s, and the
analysis was continued for 29 s.

Figure 10 depicts the fuel centerline, fuel surface, and cladding
surface temperature histories for the axial power peak elevation. As for
the 815 J/g deposition calculations, the temperatures are shown to peak
shortly after transient initiation. The magnitudes of the respective
peaks are 2870, 2080, and 2040 K. Neither the fuel nor the cladding tem-
peratures indicate melting at the fuel centerline or cladding surface.
There was no fuel or cladding melting indicated anywhere in the rod for
this energy deposition, however, the cladding surface temperature of
2040 K is very close to melting and indicates that the cladding strength
will be seriously impaired. Rod quenching at the axial power peak eleva-
tion is indicated by the sharp drop of the fuel and cladding surface tem-
peratures at about 18.5 s following the transient. The entire rod length
was quenched at about 19.5 s after transient initiation.

Figure 11 illustrates the FRAP-T4 calculated axial fuel centerline,
fuel surface, and cladding surface temperature profiles for the 1020 J/g
energy deposition. The profiles represent a time of 1.75 s after the
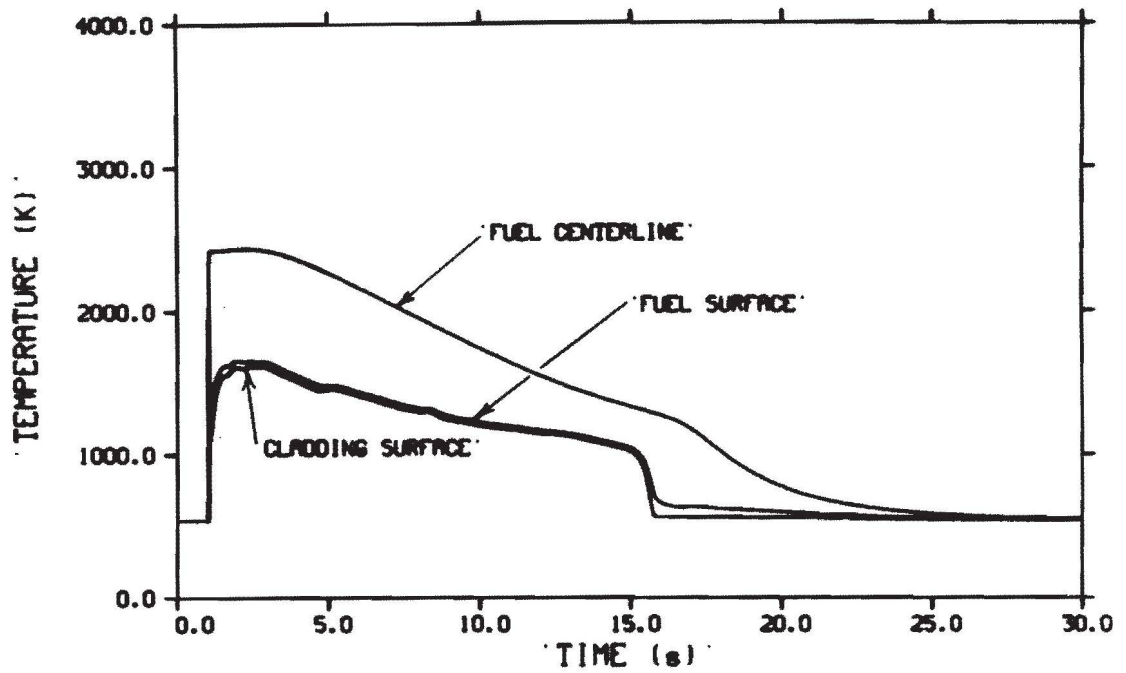
22
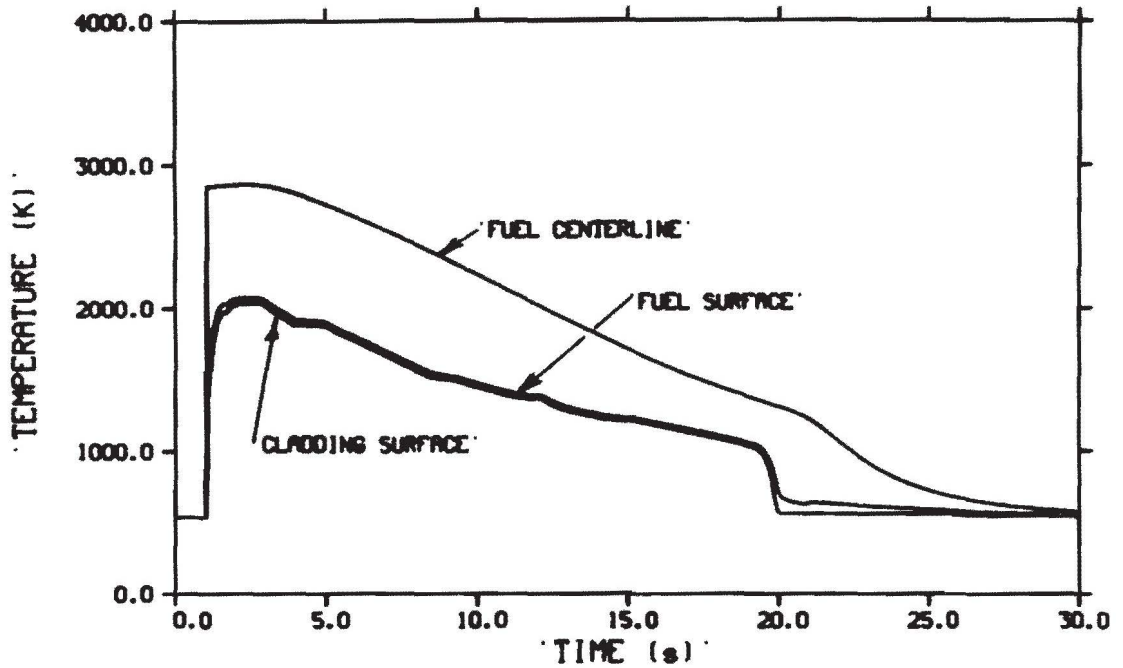
Fig. 10 Fuel rod temperature histories at the axial power peak location for a 1020 J/g pellet surface deposition.
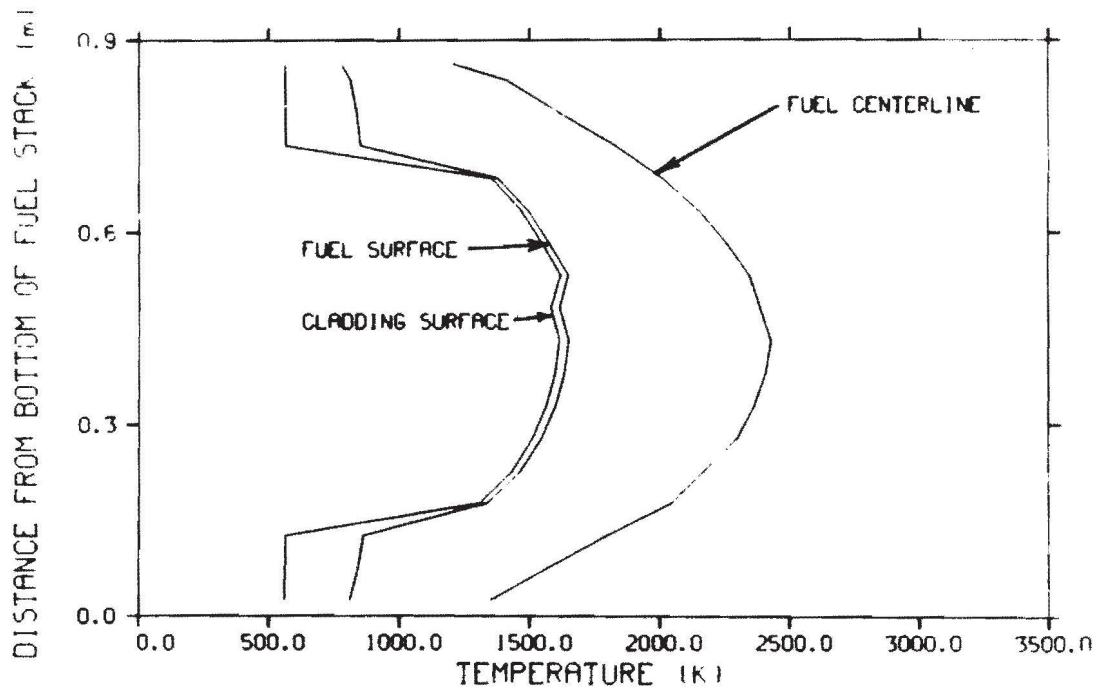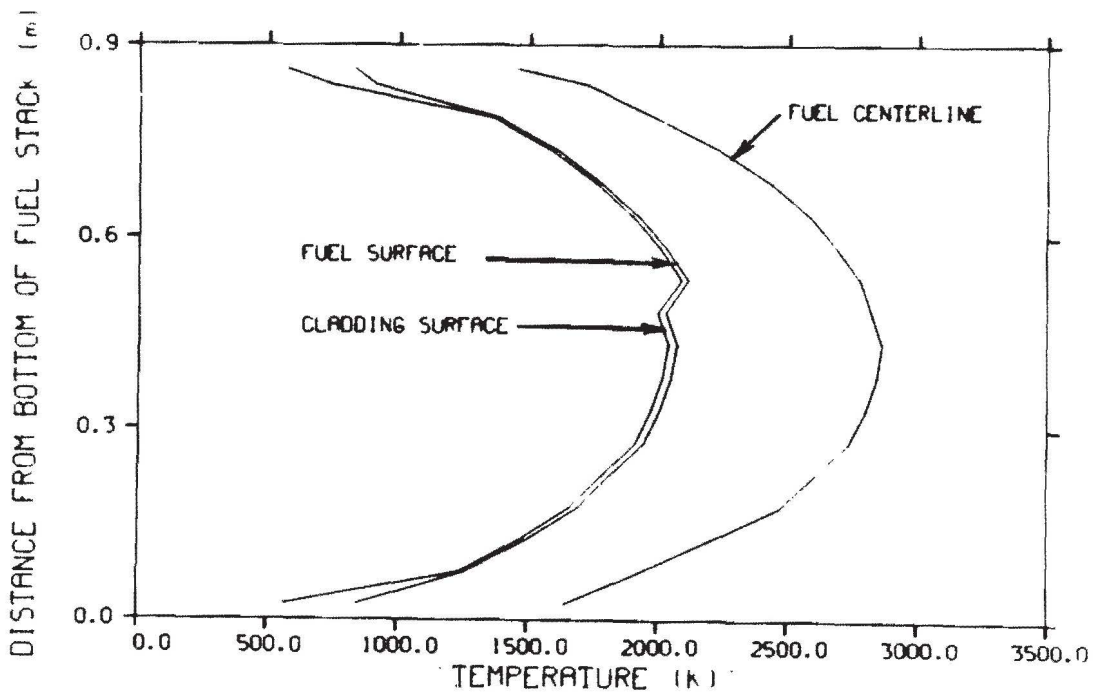

Fig. 11 Axial fuel centerline, fuel surface, and cladding surface temperature profiles at the time of the maximum cladding surface temperature for a 1020 J/g pellet surface energy deposition.
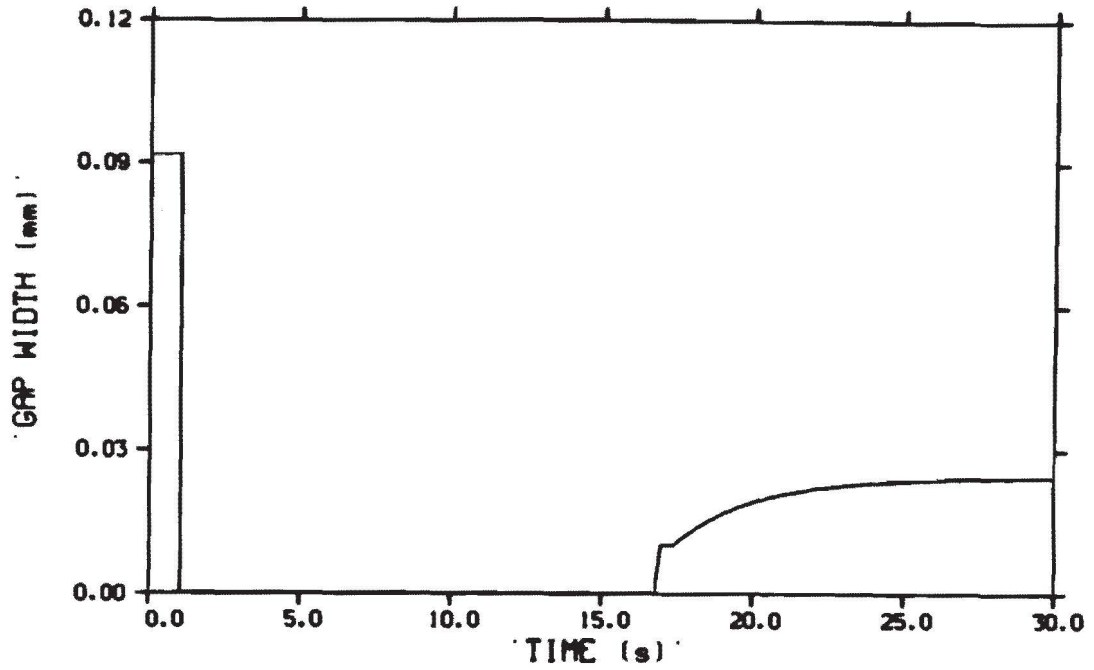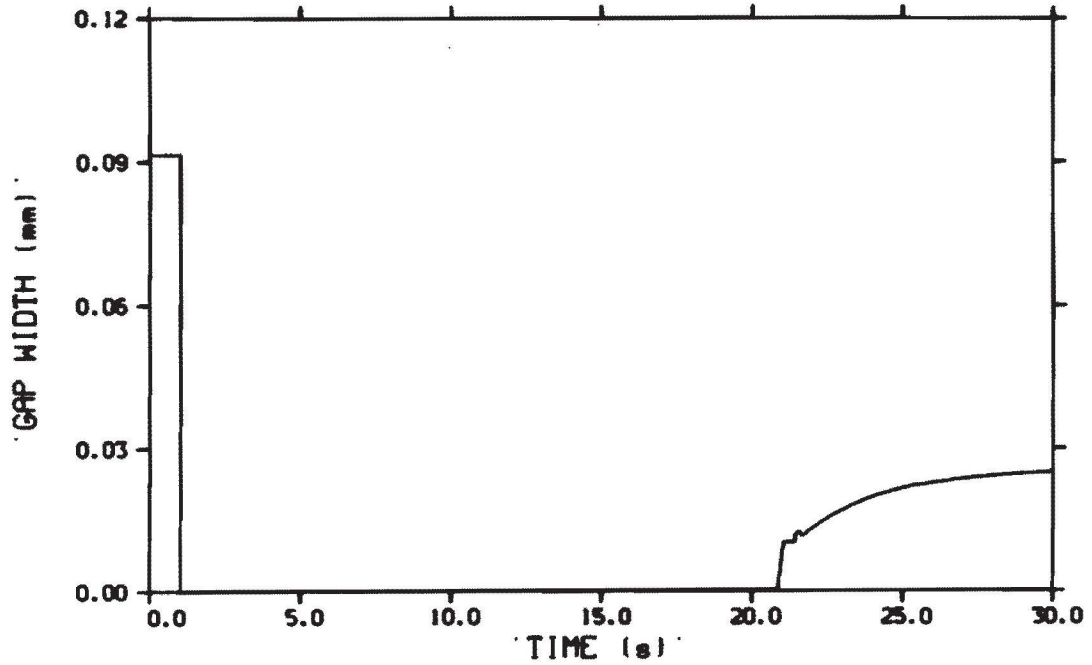
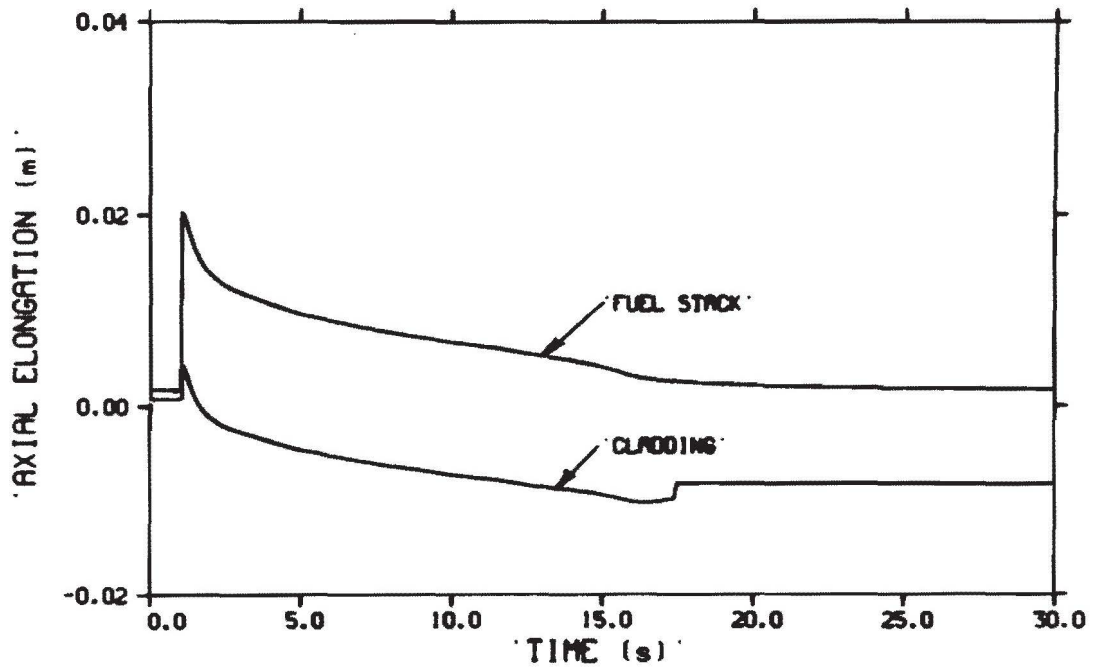Fig. 12 Fuel rod gap width history at the axial power peak location for a 1020 J/g pellet surface energy deposition.
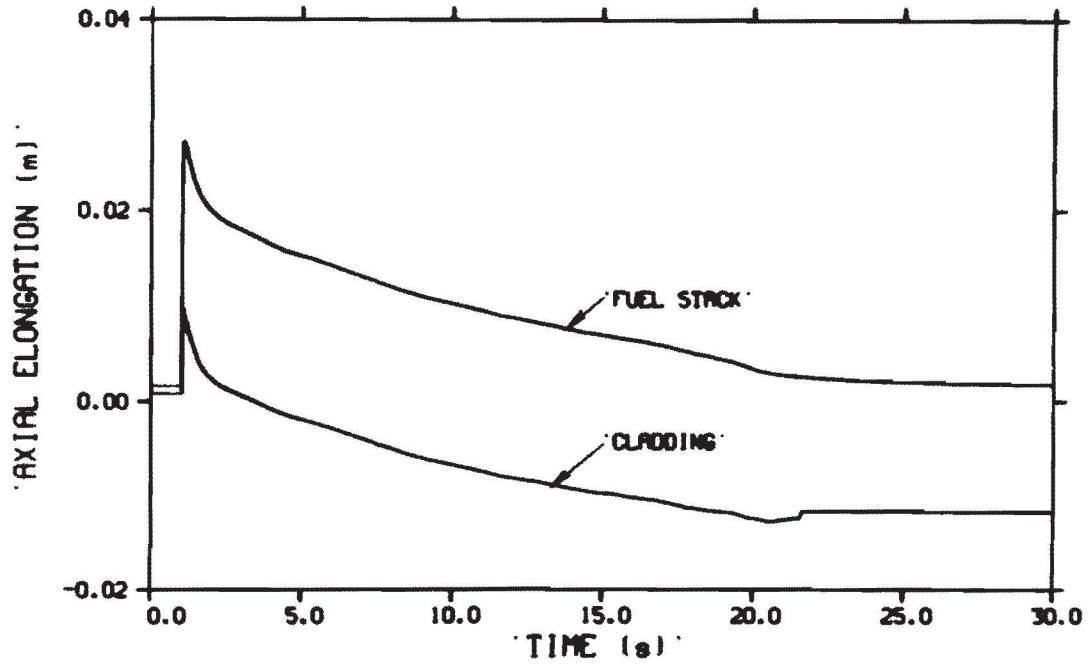
Fig. 13 Fuel stack and cladding axial elongation histories for a 1020 J/g pellet surface energy deposition.

start of the power transient when the cladding surface temperature is maximum. They demonstrate that essentially the whole length of the fuel stack was in the film boiling mode at this time. The FRAP-T4 calculations further indicated that film boiling spread over the fuel stack length immediately following the power transient.

Figure 12 shows that the fuel-cladding gap for the fuel rod closes shortly after initiation of the power transient. The pre-transient gap was 0.092 mm. The gap remains closed for almost 20 s at which time it reopens, increasing first to 0.010 mm. This reopening is a result of rod quenching. The fuel-cladding gap then continues to open asymptotically to 0.025 mm.

Fuel stack and cladding axial elongation is illustrated by Figure 13. Again, as in the lower energy deposition analysis, the cladding elongation is forced to follow that of the fuel stack while the fuel-cladding gap is closed. Shortly after 20 s, when the gap reopens, the cladding "spring back" is indicated. The magnitudes of the elongation peaks are 27.2 and 9.6 mm, corresponding to changes of 25.5 and 8.8 mm in the pre-transient lengths. The final cladding length is predicted by FRAP-T4 to be 11.8 mm shorter than its initial cold length. Again, instead of this axial cladding shrinkage, fuel pellet separation is expected to occur.

3.3.3 FRAP-T4 Calculations for a Pellet Surface Energy Deposition of 1225 J/g. The results of the FRAP-T4 analysis for a 1225 J/g energy deposition are illustrated by Figures 14 through 17. In this case, the power transient was initiated at 1.0 s and run for 26 s.

Figure 14 depicts the axial fuel centerline, fuel surface, and cladding surface temperature histories at the axial power peak elevation of the fuel rod. The respective temperatures reach maximum values almost immediately after the start of the power transient. The indicated peak fuel centerline temperature is the UO_2 melting point of 3113 K. The peak fuel surface temperature is 2175 K, and the peak cladding surface
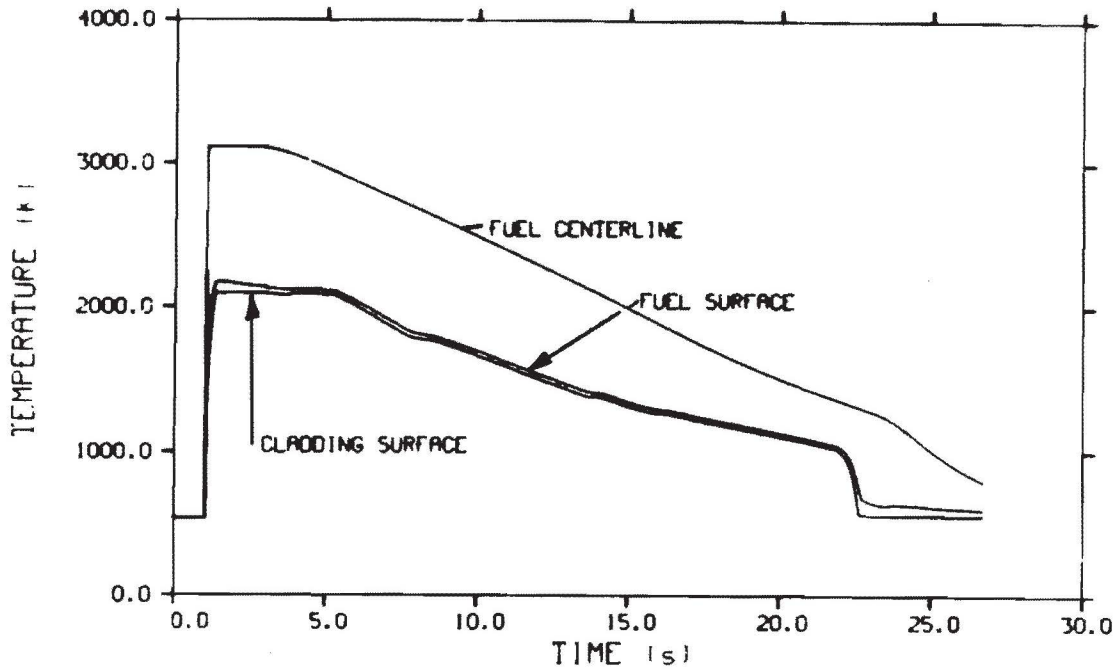
Fig. 14 Fuel rod temperature histories at the axial power
peak location for a 1225 J/g pellet surface energy deposition.
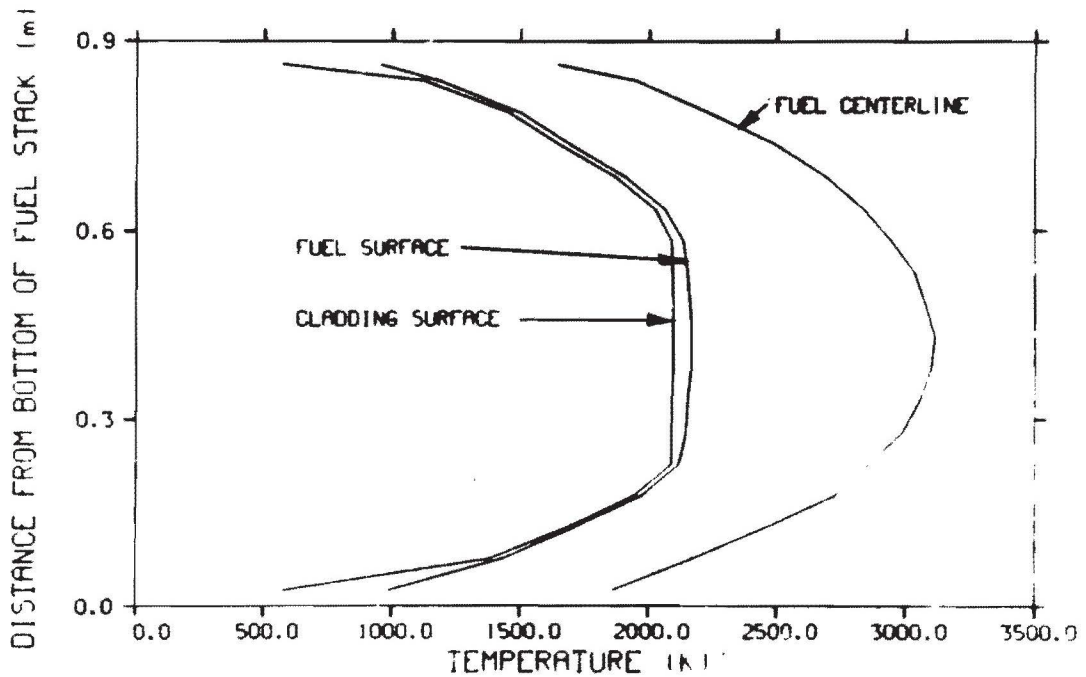
Fig. 15 Axial fuel centerline fuel surface, and cladding
surface temperature profiles at the time of the maximum
cladding surface temperature for a 1225 J/g pellet surface
energy deposition.
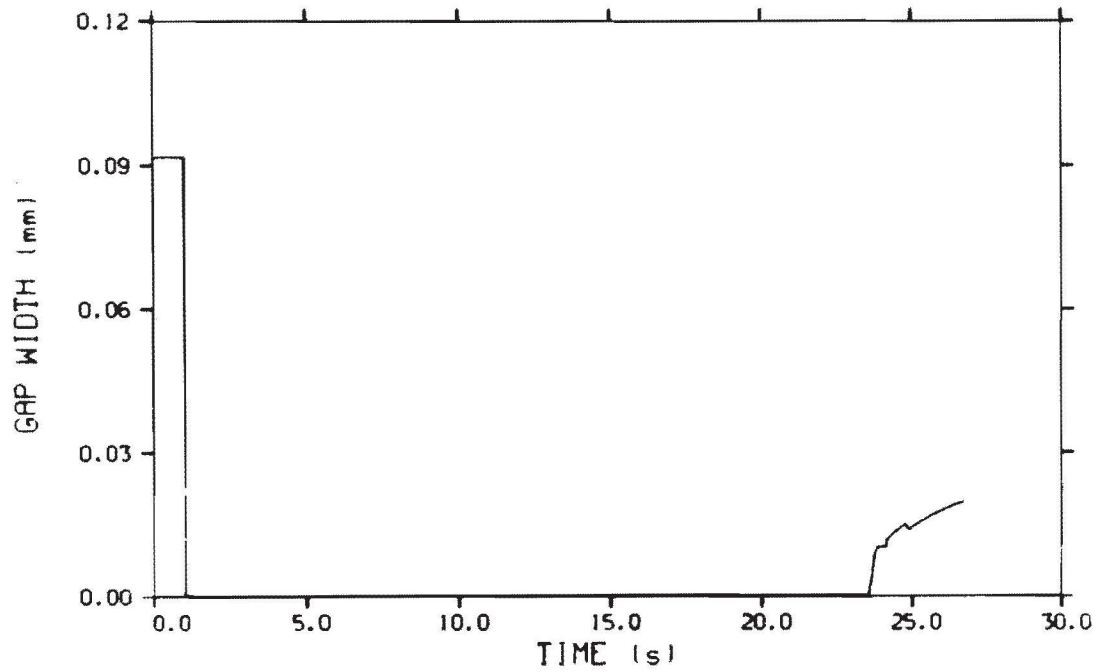
Fig. 16 Fuel rod gap width history at the axial power peak
location for a 1225 J/g pellet surface deposition.
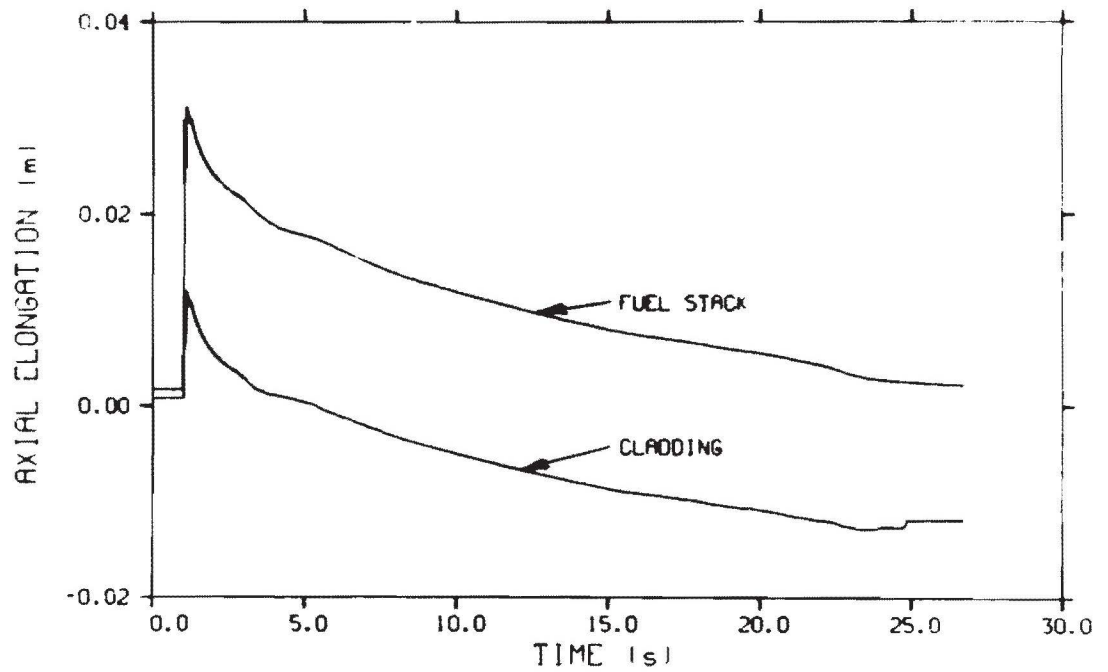
Fig. 17 Fuel stack and cladding axial elongation histories
for a 1225 J/g pellet surface energy deposition.

temperature is 2098 K, the melting temperature for zircaloy. FRAP-T4
indicated that incipient fuel melting occurs first at 0.05 s into the
transient at a fuel pellet radius of 3.5 mm and an elevation above the
bottom of the fuel stack of 0.43 m. The percentage of molten fuel
reaches a maximum value of 5.6% at 0.07 s into the transient with a
maximum fuel melt radius calculated to be 3.5 mm or 85% of the initial
fuel pellet radius. The fuel at the centerline resolidifies after 1.73 s.
Incipient cladding surface melting occurs at 0.65 s after transient ini-
tiation. Approximately 35% of the rod experiences cladding surface melting
with the entire surface resolidifying again in less than 1.35 s. At ap-
proximately 21.5 s the pellet and cladding surface temperatures, as illus-
trated by Figure 14, drop sharply indicating quenching of the rod at the
axial power peak elevation. The fuel rod is completely quenched at about
22.5 s after the transient initiation.

Figure 15 illustrates the axial fuel centerline, fuel surface, and
cladding surface temperature profiles for the 1225 J/g pellet surface
energy deposition. The profiles represent a time of 1.65 s after ini-
tiation of the transient when cladding surface temperature is at the
maximum. The temperature curves indicate that the film boiling region
extends over nearly the entire rod length at this time. The FRAP-T4
calculations further indicate that film boiling spreads over the entire
rod length almost immediately following the start of the power transient.

The fuel-cladding gap, as illustrated by Figure 16, closes almost
immediately. The pre-transient gap was 0.092 mm. It opens approxi-
mately 22.5 s later, jumping first to 0.010 mm at the time of rod quench.
After the initial increase, the gap width continues to increase asympto-
tically, reaching 0.020 mm by the time the calculations are halted. If
the calculations had continued, it is believed that the final value of the
gap width would have been approximately 0.025 mm, as it was for the lower
energy depositions.

Figure 17 illustrates the axial elongation of the fuel stack and
cladding as calculated by FRAP-T4. The two curves are similar to those

28

for the lower energy depositions. The peak magnitudes are 29.7 mm
for the fuel stack and 11.4 mm for the cladding, corresponding to
changes of 28.0 and 10.6 mm in the pre-transient lengths. The curves
remain parallel until the fuel-cladding gap reopens at approximately
24.5 s after transient initiation. After the gap opens the cladding
retains 11.9 mm of permanent shrinkage. Again, this shrinkage is not
anticipated to actually occur. Instead, fuel pellet separation is
expected.

3.3.4 <u>Fuel Radial Temperature Profile.</u> The fuel rod radial power
profile presented in Section 3.1 indicates that during the power tran-
sients the maximum energy deposition will be at the fuel pellet outer
surface. Because of this, the peak fuel temperatures calculated by
FRAP-T4 do not occur at the fuel centerline. Instead, the combination
of maximum energy deposition occurring at the pellet surface and the
normal heat flux out of the pellet surface combine to locate the peak
fuel temperatures at outer radial locations which vary with time.
Figure 18 presents the radial temperature profiles for the 815, 1020,
and 1225 J/g energy depositions. The time represented by each profile
corresponds to that which yields the maximum peak-to-centerline tempera-
ture ratio.

As illustrated in Figure 18, the peak fuel temperatures are shown to
be located at approximately 84% of the pellet radius for the 815 J/g
energy deposition, 87% of the pellet radius for the 1020 J/g deposition,
and 89% of the pellet radius for the 1225 J/g deposition. The peak-to-
centerline temperature ratios for the three cases are, respectively,
1.07, 1.06, and 1.05.

3.3.5 <u>Cladding Temperature versus Peak Energy Deposition.</u>
Figure 19 is a plot of the maximum cladding temperatures versus peak
pellet surface energy depositions for the three 9.70 mm OD fuel rod
behavior analyses discussed in Sections 3.3.1, 3.3.2, and 3.3.3, and

29
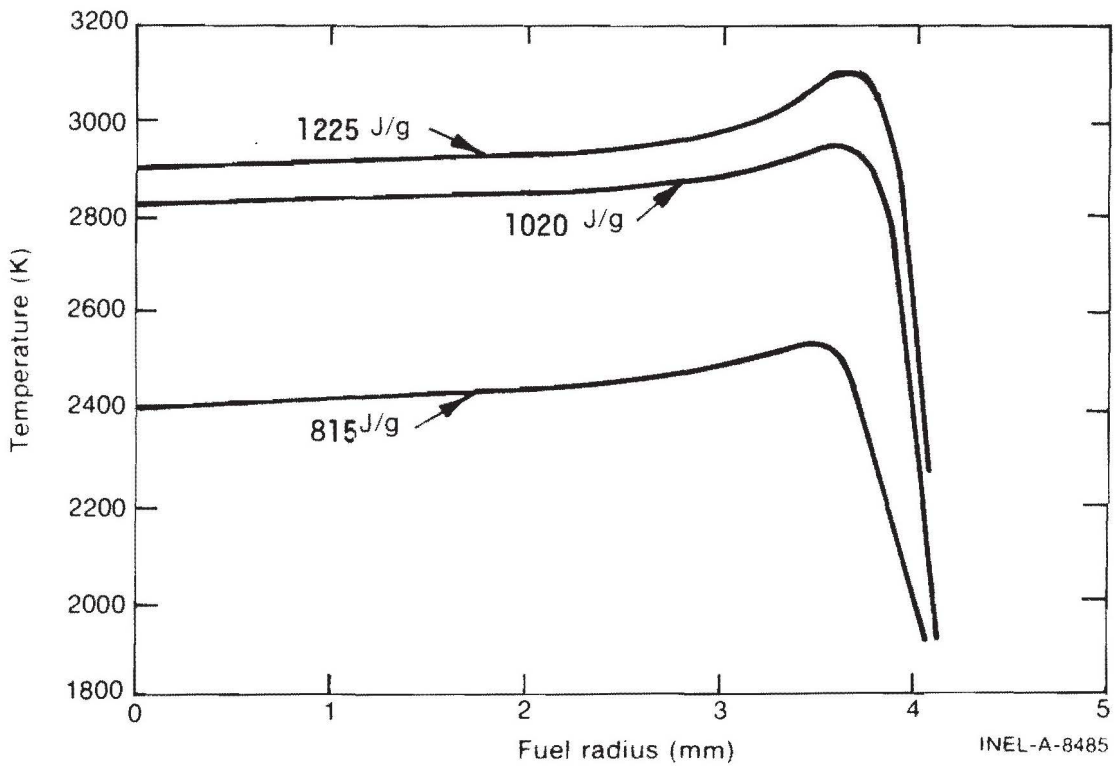
Fig. 18 Radial temperature profiles of fuel at time corresponding to peak centerline temperature for pellet surface energy depositions of 815, 1020, and 1225 J/g.
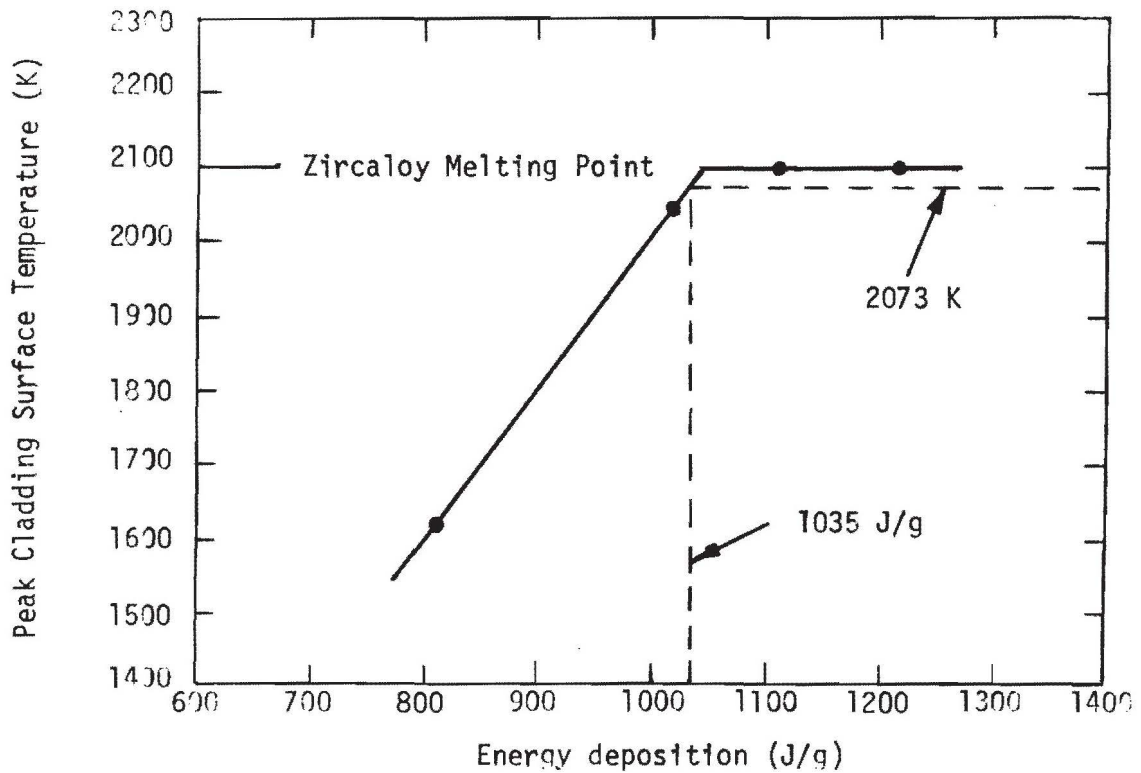
Fig. 19 Peak cladding temperature as a function of pellet surface energy deposition.

an additional analysis that was not presented[a]. The curve illustrates the effect of pellet surface energy deposition on maximum cladding temperature and, therefore, the likely energy deposition failure threshold. This indicates that, based on FRAP-T4 calculations, a pellet surface energy deposition of 1045 J/g (250 cal/g) at the axial power peak elevation results in incipient cladding surface melting at the power peak elevation for the 9.70 mm OD fuel rods. A pellet surface energy deposition of 1035 J/g (247 cal/g) corresponds to a peak cladding temperature of 2073 K. It is believed that at 2073 K, the cladding will be weak enough to fail due to low pressure cladding rupture. This limit was chosen based on the results of the previous RIA tests which will be discussed in Section 4.

3.3.6 FRAP-T4 Calculations for a Radially Averaged Energy Deposition of 2510 J/g.

This case was run to provide baseline data for predicting the mode of failure for the final high energy phases of the Scoping Test (RIA-ST-4 and RIA-ST-5). These two phases of the Scoping Test are non-programmatic and intended to address PBF safety concerns.

The 10.73 mm OD fuel rod, according to FRAP-T4 will undergo extensive disintegration by melting as a result of the 2510 J/g radially averaged energy deposition. Incipient rod failure was indicated at 0.035 s as the result of cladding overstress induced by pellet-to-cladding interaction. At 0.075 s, 60% of the total fuel volume had passed the melting point with 55% of the axial length of the fuel stack beyond it. A maximum fuel temperature of 4950 K was reached. Incipient cladding surface melting was indicated at 0.08 s, and 64% of the axial surface length was molten at 0.236 s. FRAP-T4 does not have a UO_2 vapor pressure model at present, thereby precluding the calculations from indicating this expected failure mechanism.

---

[a] A similar FRAP-T4 analysis was made at 1120 J/g but was run only long enough to determine peak cladding surface temperature. The results indicated cladding melting.

31

3.4 Cladding Embrittlement Analysis

Past test experience with high temperature cladding oxidation has provided two criteria for evaluating the likelihood of rod failure, due to cladding embrittlement, based on reaction layer thicknesses. To use these criteria, the FRAP-T4 predicted cladding surface temperature histories for the 815, 1020, and 1225 J/g pellet surface energy depositions were used to run three BUILD5 computer code calculations. The BUILD5 code applies the Cathcart correlation[6] to calculate zircaloy one-side reaction layer thicknesses when given a surface temperature history. Although the FRAP-T4 histories exceed the cladding temperature range of the BUILD5 code, it was used as the only available method of evaluating the cladding embrittlement failure mode. The BUILD5-calculated reaction layers used in the cladding failure criteria are the outer ZrO_2 and oxygen-stabilized alpha layers (α- layer). Fuel-cladding contact following the energy depositions causes the formation of another oxygen-stabilized alpha layer on the inside surface of the cladding. The thickness of this inner alpha layer can be approximated by that of the outer layer. This approximation is based on the postirradiation examination of numerous cladding specimens.

Doubling the BUILD5 predicted alpha layer thickness and adding the ZrO_2 layer thickness, yields an approximation of the total expected cladding participation in the reaction process. For the 815, 1020, and 1225 J/g energy depositions respectively, the total thickness of the reaction layers are;

(1) ZrO_2 = 0.013 mm and α = 0.032 mm,
(2) ZrO_2 = 0.043 mm and α = 0.150 mm, and
(3) ZrO_2 = 0.072 mm and α = 0.280 mm.

The two criteria for rod failure during reactor operation, due to high temperature cladding oxidation, can be expressed by the inequalities:

(1) F(w) < 0.62, and
(2) ECR > 17%.

32

The first criterion indicates that when the fraction of the original cladding thickness that has remained in the beta phase $F(w)$ becomes less than 0.62, cladding failure due to embrittlement can be expected. "$F(w)$" can be calculated from the reaction layers using the equation;

$$F(w) = (Th - \alpha - \frac{ZrO_2}{1.54}) / Th$$

where,

Th = the original cladding thickness,

α = the total alpha layer thickness, and

ZrO_2 = the ZrO_2 layer thickness.

The second criterion indicates that when the ECR ratio (equivalent cladding thickness reacted to form ZrO_2-to-the oxygen weight fraction in the alpha layers) is greater than 17%, cladding failure due to embrittlement can be expected. "ECR" can be calculated from the reaction layers using this equation;

$$ECR = \frac{1}{Th} \left[\frac{ZrO_2}{1.54} + \frac{\alpha}{1.54\sigma} \right] \times 100,$$

where, σ is a factor relating the ratio of oxygen-to-zircaloy in ZrO_2 (1.54) to that ratio in oxygen-stabilized alpha-zircaloy; "σ" was approximated to be a constant value of 5.3.

Table IV presents the results of applying these two criteria to the BUILD5-derived reaction layer thicknesses for the 815, 1020, and 1225 J/g energy depositions. The table further indicates that, based on the "$F(w)$" criteria, the 1225 J/g pellet surface deposition will provide a cladding surface temperature history that can be expected to result in sufficient cladding embrittlement to induce failure. Figure 20 is a plot of the BUILD5-derived "$F(w)$" values provided by Table IV, indicating that the minimum pellet surface energy deposition that will result in embrittlement-induced cladding failure is 1110 J/g (265 cal/g). This result, combined with the previous indication (Section 3.3.5) that the failure threshold will be 1035 J/g with a maximum cladding temperature

33

TABLE IV

REACTION LAYER CLADDING FAILURE CRITERIA RESULTS FOR 815, 1020, AND 1225 J/g PELLET SURFACE ENERGY DEPOSITIONS

Energy Deposition (J/g)	F(w) [a]	ECR[b] (%)
815	0.94	1.9
1020	0.72	7.2
1225	0.49	12.7

[a] Rod failure indicated if less than 0.62.
[b] Rod failure indicated if greater than 17%.
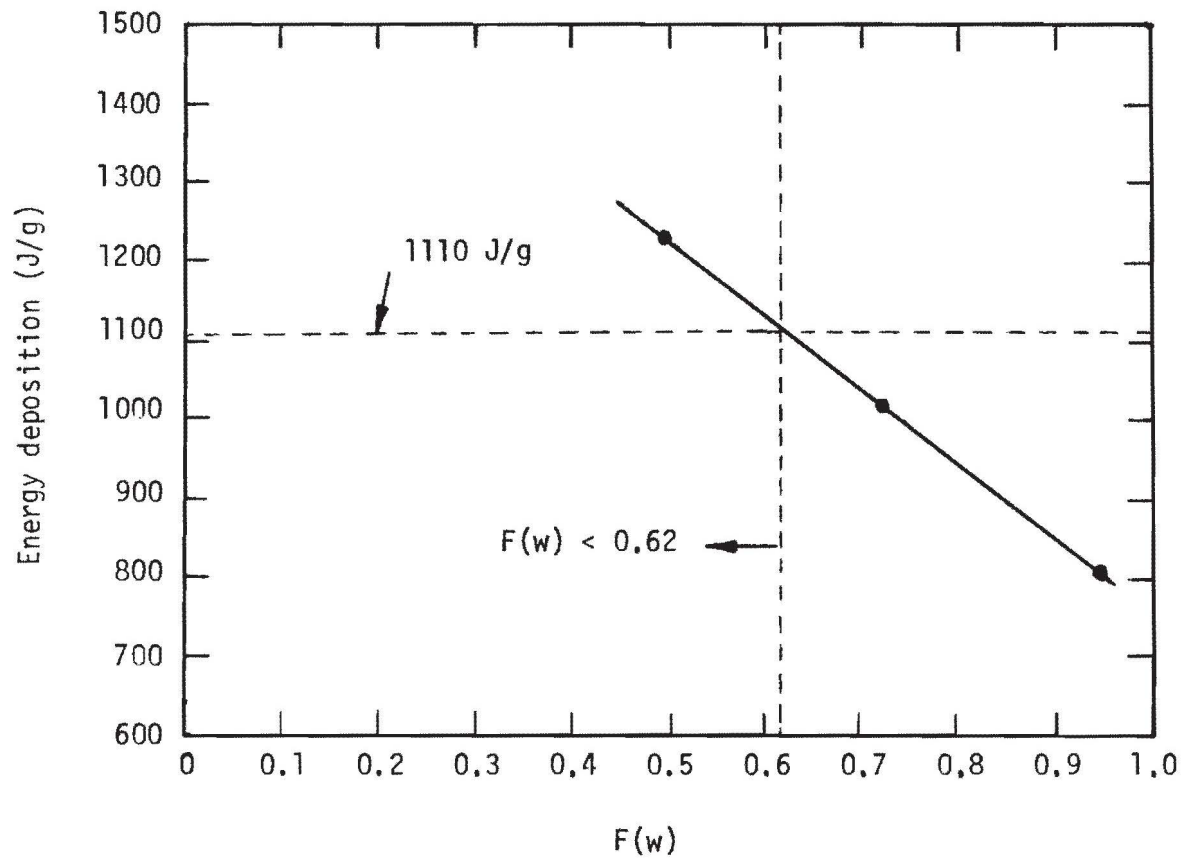
Fig. 20 Fraction of the original cladding thickness that has remained in the beta-zircaloy phase with respect to pellet surface energy deposition.

should be rupture due to high temperature weakening of the cladding and not brittle fracture.

3.5 Pressure Pulse Analyses

The analyses discussed in this section were performed to provide baseline data for predicting the magnitudes of generated pressure pulses for the final high energy phases of the Scoping Test.

Pressure pulses are expected to result from fuel rod failure and possible subsequent fuel-coolant interactions during the 1990 and 2510 J/g radially averaged energy depositions of RIA-ST-4 and RIA-ST-5. The magnitudes of these pulses were calculated using the SPIRT computer code. The SPIRT code calculated the generation of super heated steam by molten fuel particles, resulting in rapid pressurization. The method modeled coolant compression within the IPT without including the acoustic filters or thermal swell accumulators.

A single fuel rod with an active length of 0.914 m, a cladding OD of 10.73 mm, and a flow shroud ID of 16.3 mm was considered in both the 2500 and 1990 J/g cases. The initial coolant conditions were 538 K, 6.45 MPa, and 490 kg/s-m^2 (85 cm^3/s). Fuel fragmentation weight distribution and particle sizes for the SPIRT computer code calculation were obtained from the results of the SPERT CDC tests. A fuel dispersal time of 1 ms was used.

The SPIRT calculation for the 2510 J/g deposition rod failure case yielded a source pressure of 24.8 MPa with pressure doubling occurring at the top and bottom of the IPT. The pressure wave propagation back and forth through the IPT gave a maximum pressure of 34.5 MPa with a rise time of 7 ms. The 1990 J/g deposition rod failure resulted in a calculated pressure pulse of 24.1 MPa with the SPIRT code. SPIRT predicted a pressure doubling of 31.7 MPa at 7 ms after fuel dispersal.

4. RESULTS OF PREVIOUS RIA TESTS

The applicable experimental data on fuel rod behavior, simulating an RIA, have been obtained from programs carried out in the SPERT Capsule Driver Core (CDC) and TREAT facilities[a]. An ongoing test program at the NSRR[b] is providing additional applicable data. In each of these facilities, encapsulated oxide fuel with metal cladding was subjected to power transients comparable to those of hypothetical RIAs in light water reactors. The test capsule generally contained stagnant water at atmospheric pressure and room temperature.

Results from these tests have shown that the most important aspect of an RIA or an RIA test, is the magnitude of energy deposited into the fuel[7]. In RIA experiments of the type carried out in SPERT-CDC and NSRR, the energy deposited near the outside edge of the pellet is the primary heat source for cladding melting, while the energy deposited in the interior of the fuel is not conducted to the cladding surface until after the maximum cladding surface temperature is reached. The effects of differences in fuel density can be taken into account by converting the energy deposition data to a volumetric basis. It was found that the failure threshold behavior of various test fuels could be considered in terms of peak energy deposition per unit volume of fuel at the fuel surface, a parameter that should be strongly related to cladding temperature. Figure 21 shows the failure behavior data obtained from the SPERT-CDC and NSRR tests when plotted in terms of fuel surface energy deposition per unit volume. Taking into account the uncertainty in the energy deposition determination of the NSRR data, the combined data indicate the existence of a single failure threshold. With the exception of the GEP-pellet rods, all other rods failed when the peak energy deposition

---

[a] SPERT is the acronym for Special Power Excursion Reactor Tests, the name given to test facilities at the Idaho National Engineering Laboratory. TREAT is the acronym for Transient REActor Tests, another INEL facility.

[b] NSRR stands for Nuclear Safety Research Reactor, a facility of the Japan Atomic Energy Research Institute.
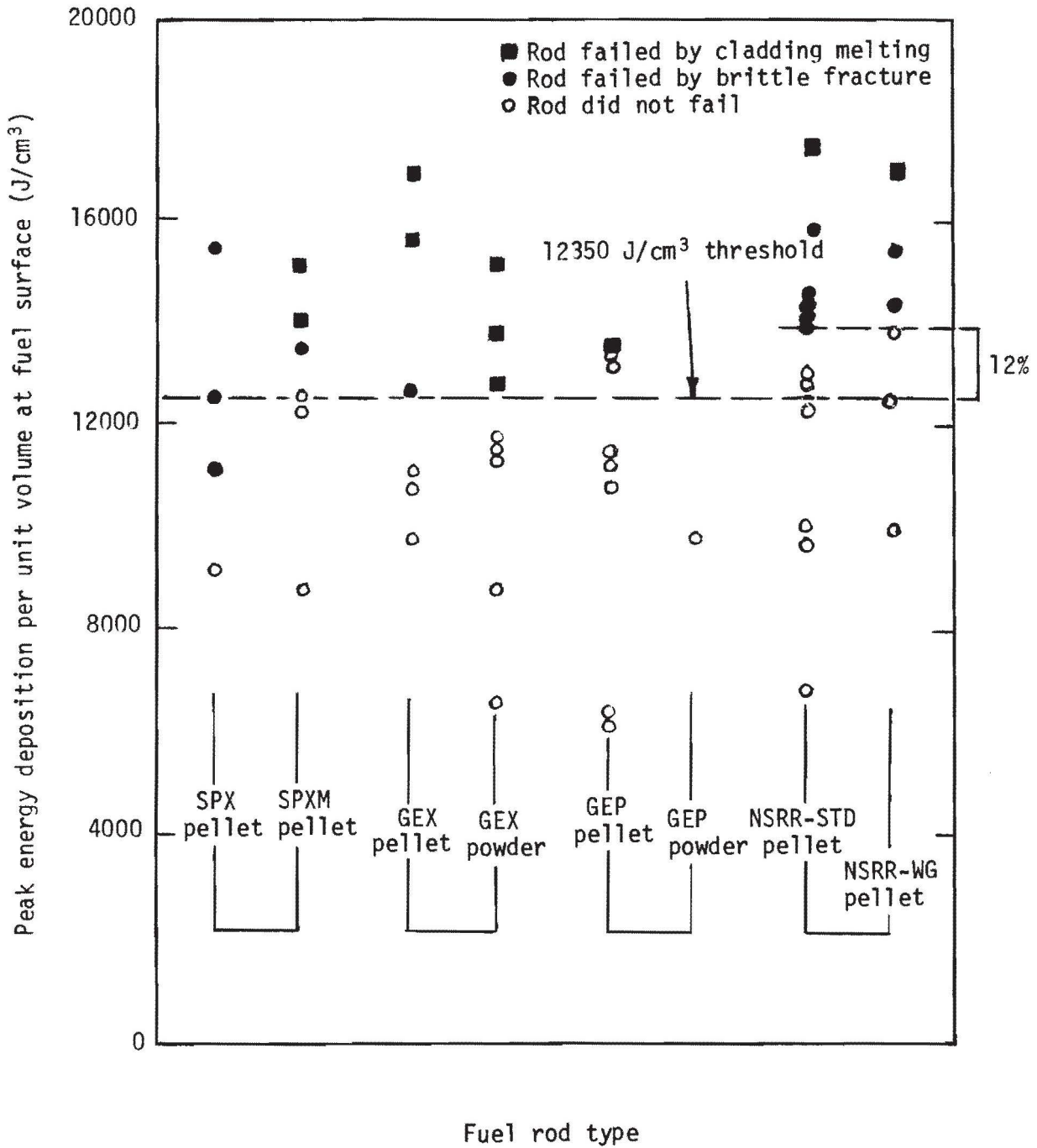
Fig. 21 Failure behavior of CDC and NSRR test fuel rods as a
function of pellet surface energy deposition per unit fuel
volume.

near the fuel surface exceeded 12.350 x 10^3 J/cm^3 (2950 cal/cm^3).
Conformity to this rule should apply as long as there is fuel-cladding
gap closure following the transient. When the RIA-ST-1, -2, and -3 fuel
density of 10.365 g/cm^3 is considered, the failure threshold becomes
1190 J/g (284 cal/g).

Figure 21 also provides information about the failure modes of the
various fuel types. With the exception of the GEP rods, all pellet rods
failed by brittle fracture at energy depositions near the theshold value.
At slightly higher energy depositions, the failure mode changed to low
pressure rupture due to weakening of the cladding as the melting temper-
ature was approached (for all pellet rods except the SPX type). The
failure mode of the SPX pellet rods is believed to have been influenced
by their unusual dimensional characteristics which result in stronger
pellet-cladding interaction and larger bending forces. Based only on
this information, the failure of the RIA-ST, 9.70 mm OD test rods could
be postulated to result from brittle fracture for energy depositions
near the theshold value and low pressure rupture due to high temperature
cladding weakening for slightly higher depositions. The high coolant
system pressure of the PBF in-pile tube will have some effect on the low
pressure cladding rupture failure mode. The nature of this effect is
unknown at present. Small internal rod pressure increases were suffi-
cient to cause cladding rupture in previous tests conducted at atmo-
spheric pressure. For energy depositions greater than 1465 J/g the
failure mode observed in the SPERT-CDC tests was vigorous cladding
rupture prior to melting probably due to internal UO_2 vaporization
pressure.

Figure 22 shows the maximum cladding surface data from the SPERT-CDC
and NSRR data displayed as a function of peak energy deposition per unit
volume at the fuel surface. With one exception, fuel rod failures occurred
only when cladding temperatures exceeded a temperature of 2073 K, 25 degrees
below the melting point of zircaloy (2098.2 K). For this reason, 2073 K,
was chosen as the failure limit for the FRAP-T4 results discussed in
Section 3.3 and illustrated by Figure 19. The excellent correlation between
cladding temperature and rod failure can be expected because of the direct
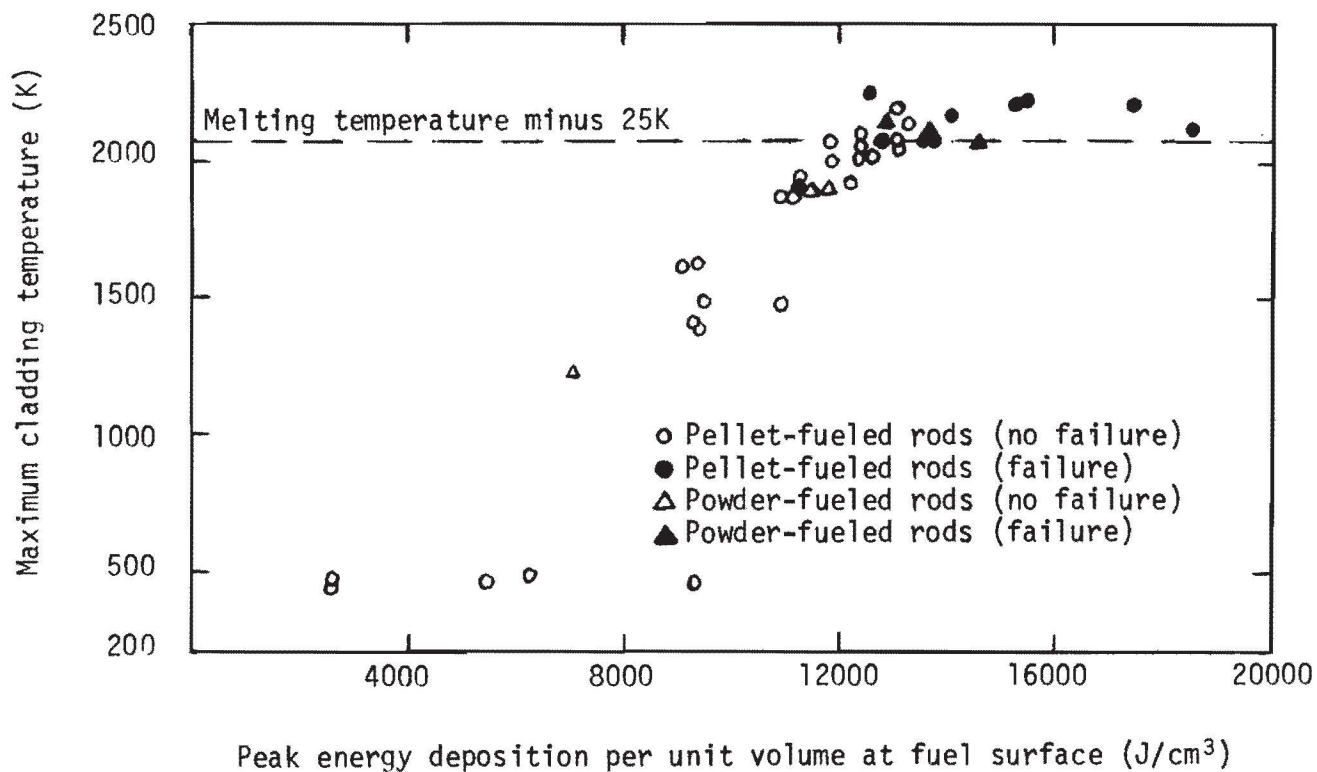
Fig. 22 Maximum cladding temperature as a function of pellet surface energy deposition per unit fuel volume for the CDC tests.

relationship between fuel surface energy deposition and cladding temperature and the postulated existence of an energy deposition failure threshold.

The amount of energy deposition during a test transient also affected the consequences of failure in unirradiated UO_2 fuel rods. Increasing energy depositions resulted in more severe fuel rod damage and larger measured capsule pressures. The extent of metal-water reaction and conversion from nuclear-to-mechanical energy also increased. Cladding and fuel deformed both radially and axially. The radial deformation was directly related to thermal expansion of the fuel. Elongation of the cladding was apparently due to growth of the fuel stack following fuel-cladding gap closure. Slippage between the cladding and the fuel was also observed.

Recent tests at the NSRR have also addressed the possible effects on rod failure of repetitive testing on the same fuel rod. These tests have not provided conclusive data yet but preliminary results indicate that the repetitive transients have little effect on failure threshold. Reduction of the fuel-water ratio through the use of flow shroud enclosures (no forced flow) caused a reduction in the failure threshold by about 10% in some tests at the NSRR.

5. CONCLUSIONS

Thus far, this report has presented the results of several different analyses and a discussion of some previously obtained RIA test results. It is the purpose of this section to evaluate the information presented and arrive at experiment predictions for the RIA Scoping Test. First, test fuel rod energy as a function of PBF reactor core energy is predicted for the 9.70 mm OD fuel rods of phases RIA-ST-1, RIA-ST-2, and RIA-ST-3. The pellet surface energy deposition at which the 9.70 mm OD fuel rods are expected to fail and the expected mode of failure are predicted next. Finally, the mode of failure for the 10.73 mm OD test fuel rods subjected to radially averaged energy depositions of 1990 and 2510 J/g and the magnitudes of the expected failure-induced pressure pulses are predicted. The conclusions which have been drawn to make these predictions are based on the respective analyses and the SPERT, TREAT, and NSRR Test results.

The prediction of test fuel rod energy with respect to core energy is based on the results of the reactor physics calculations discussed in Section 3.1. Table III, in that section, provides the results of the calculations and thus the predictions. The radial fuel pellet surface-to-average power factor is expected to be 1.076.

The prediction of energy deposition failure threshold and mode of failure for the 9.70 mm OD fuel rods is based primarily on the results of the fuel rod behavior and cladding embrittlement analyses discussed in Sections 3.3 and 3.4. Previous RIA testing experience, such as that obtained in the SPERT-CDC and NSRR facilities, serves to direct and provide a comparison with the predictions.

From the results of the SPERT-CDC and NSRR Tests (discussed in Section 4), three principal conclusions can be drawn. First, a maximum cladding temperature reaching or exceeding 2073 K should result in cladding failure following a reactivity insertion transient. Second, the mode of failure should be either brittle fracture of the cladding due to

42

excessive oxidation or pressure-induced rupture due to high temperature weakening of the cladding. Finally, for RIA-ST, 9.70 mm OD-type fuel rods, the baseline data indicate that the minimum energy deposition at the pellet surface resulting in rod failure should be 1190 J/g (284 cal/g) for transients initiated from ambient coolant conditions and no forced flow. The PBF-RIA tests will be performed with initial conditions of 538 K, 6.45 MPa, and 85 cm^3/s. The fuel enthalpy associated with this 240 K difference in initial temperature is equivalent to a pellet surface energy deposition of about 69 J/g. If the previous CDC and NSRR power transient tests had been run with the PBF-RIA test initial conditions, the observed failure threshold would be expected to drop to 1122 J/g (268 cal/g), neglecting the thermal-hydraulic effects of coolant flow and flow shrouding.

FRAP-T4 calculations showed that a pellet surface energy deposition of approximately 1035 J/g (247 cal/g) will result in a maximum cladding temperature of 2073 K for the 9.70 mm OD fuel rods. From the CDC-NSRR results it would be expected that this temperature will cause cladding failure. The cladding embrittlement analysis precludes brittle fracture as the mode of failure, indicating that the accumulation of oxygen into the zircaloy would not be sufficient after the 1035 J/g energy deposition to make this failure mode probable. The expected failure mode, therefore, is rupture due to high temperature weakening of the cladding, and it should occur when the cladding temperature is at a maximum. The consequences of this mode of failure are expected to be minimal with only small pressure pulses generated.

The energy deposition threshold predicted from the analyses (1035 J/g) is 87 J/g (21 cal/g) less than the 1122 J/g of the previous RIA tests. It is believed that this discrepancy is a result of uncertainty in the complex transient heat transfer correlations of FRAP-T4 and possibly the influence of the PBF-RIA test flow shrouds. It should also be stated that uncertainty exists in the cladding embrittlement analysis because the temperatures considered were beyond the range of reliability of the reaction layer correlation, and because the failure criteria were based on power-coolant-mismatch tests and not RIAs. The SPERT-CDC tests

43

results indicate that the failure mode for the initial RIA-ST phases could be brittle fracture due to cladding oxidation. The presence of a flow shroud increases the time to cladding quench without greatly affecting the peak cladding temperature. This should result in a higher probability of cladding embrittlement failure.

The mode of failure for the 10.73 mm OD fuel rods used in phases RIA-ST-4 and RIA-ST-5 and the magnitudes of the pressure pulses expected in the coolant as a result of their failure are predicted based on the FRAP-T4 calculation performed, previous experience, and the pressure pulse analyses discussed in Section 3.5. Past RIA Tests have all indicated that for high energy depositions, above 1465 J/g (350 cal/g) radially averaged, the failure mode is cladding rupture due to internal rod pressurization from UO_2 vaporization. The FRAP-T4 calculation that was performed for the 2510 J/g case indicates extensive UO_2 vaporization, supporting the previously observed failure mode. Therefore, for radially averaged energy depositions at the power peak elevation of 1990 and 2510 J/g, the rod failure mode is predicted to be cladding rupture due to internal rod pressurization from fuel vaporization.

The 2510 J/g energy deposition rod failure should result in a source coolant pressure of 25 MPa with pressure doubling occurring at the top and bottom of the IPT. The pressure propagation back and forth through the IPT will give a maximum pressure of 35 MPa with a rise time of 7 ms. The 1990 J/g deposition rod failure should result in a source pressure pulse of 24 MPa. Pressure doubling of 31.7 MPa is predicted to occur at 7 ms after fuel dispersal.

To summarize:

(1) Table III of Section 3.1 provides the predictions of test rod energy as a function of PBF core energy. The radial fuel pellet surface-to-average factor is 1.076.

(2) The energy deposition failure threshold for RIA-ST-1, RIA-ST-2, and RIA-ST-3 is predicted to be 1035 J/g, and the mode of

failure is predicted to be pressure-induced rupture due to high temperature weakening of the cladding. The generated pressure pulses are expected to be minimal for these failures.

(3) The failure mode for the high energy phases, RIA-ST-4 and RIA-ST-5, is predicted to be internal pressure induced cladding rupture due to UO_2 vaporization. The maximum dynamic pressures that will result are predicted to be 31.7 and 34.5 MPa, respectively, for the 1990 and 2510 J/g radially averaged energy depositions.

The first three phases of the RIA Scoping Test were designed to experimentally determine the failure threshold and failure mode for the 9.70 mm OD fuel rods for Boiling Water Reactor hot startup conditions. The data obtained from these transients will be valuable in refining the analytical codes used to make these predictions. These data will point out deficiencies in the codes' abilities to characterize the RIA transient behavior, and they will identify additional areas of code development. The final phases of the Scoping Test will provide sufficient pressure pulse data to refine this calculation.

6. REFERENCES

1. R. S. Semken, T. Inabe, Z. R. Martinson, Reactivity Initiated Accident Test Series RIA Scoping Test Experiment Operating Specification, TFBP-TR-217 (May 1978).

2. T. E. Young, Physics Calculations for RIA Scoping Test, EG&G Idaho, Inc. Interoffice Correspondence, YNG-8-77 (October 1977).

3. R. S. Marsden, SCAMP Code Input Description, Mars-15-68 (May 1968).

4. K. R. Katsma et al, RELAP4/MOD5 - A Computer Program for Transient Thermal-Hydraulic Analysis of Nuclear Reactors and Related Systems User's Manual, ANCR-NUREG-1335 (September 1976).

5. J. A. Dearien et al, FRAP-T4 A Computer Code for the Transient Analysis of Oxide Fuel Rods, TFBP-TR-237 (November 1977).

6. J. V. Cathcart et al, Zirconium Metal-Water Oxidation Kinetics IV, Reaction Rate Studies, ORNL/NUREG-17 (August 1977).

7. T. Fujishiro et al, Light Water Reactor Fuel Response During Reactivity Initiated Accident Type Tests, TFBP-TR-246 (December 1977).

APPENDIX A

RIA SCOPING TEST

RELAP4 MODEL DESCRIPTION

APPENDIX A

RIA SCOPING TEST RELAP4 MODEL DESCRIPTION

The RELAP4 nodalization model is illustrated by Figure A-1. In the model, the RIA-ST test loop and in-pile tube are described by 59 fluid volumes connected by 63 flow junctions. There is a pump and heat exchanger in the loop, and there are 5 stacked heat slabs attached to the fuel region fluid volumes which represent the fuel rod. Tables A-I and A-II list the fluid volume and flow junction data used in the analysis.

In the model, the in-pile tube consists of a downcomer through which coolant enters the lower plenum. The coolant then splits and 80% of the flow bypasses the fuel rod flow shroud. The remaining 20% passes up through the turbine flowmeters and inlet orifice and flows into the fuel rod region of the flow shroud. The two coolant paths converge again in the upper plenum and then exit the in-pile tube, flowing out into the RIA-ST test loop.

The rod axial power profile that was used in the RELAP analysis is shown in Table A-III. The 1350 J/g pellet surface energy deposition transient was distributed to the fluid volumes of the model as the table indicates. In addition to the 1350 J/g deposition, moderator heating was also deposited directly into the fuel region fluid volumes. A moderator heating rate of ∿1.8% of the transient energy deposition rate in the fuel rod was modeled. Total moderator heating was about 7.88 kJ. The analysis consisted of 1 s of steady state calculation time followed by the transient. The total energy deposited into the fuel region fluid volumes was 446 kJ.
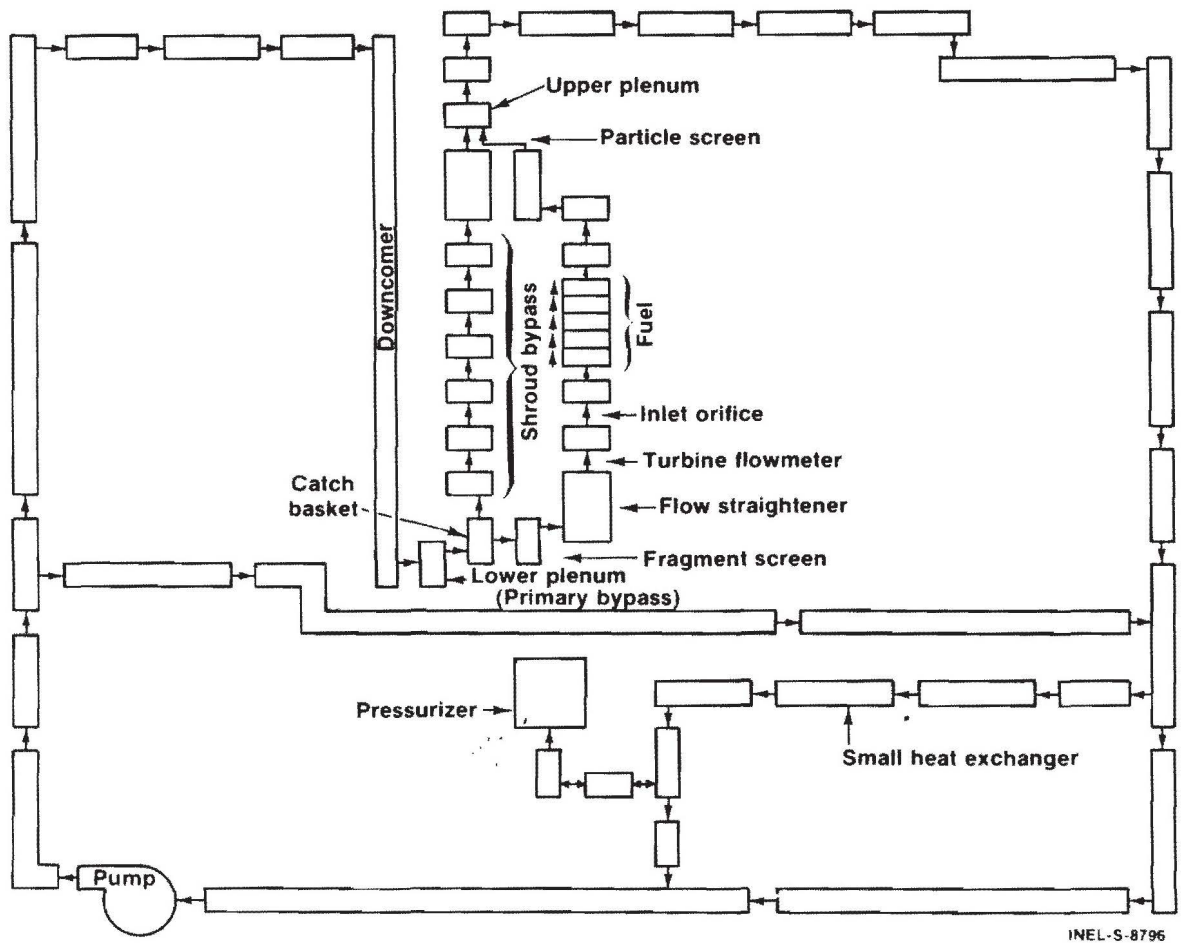
Fig. A-1 RELAP transient model of the RIA-ST test loop.

TABLE A-I

RELAP CONTROL VOLUME DATA USED IN RIA-ST-1 ANALYSIS

VOLUME NUMBER	PHYSICAL DESCRIPTION	VOLUME FT^3	FLOW AREA FT^2	STEADY-STATE PRESSURE, PSI	STEADY-STATE TEMPERATURE, F	VOLUME HEIGHT, FT	DIAMETER FT
1	Pump	.4106E+00	.7170E-01	1124.1740	509.00	1.0830	.3022
2	Piping & Line Heater	.3643E+01	.7170E-01	1311.2240	509.00	8.0000	.3022
3	Piping	.1111E+01	.7170E-01	921.0500	509.00	4.5830	.3022
4	Piping	.7170E-01	.7170E-01	919.5280	509.00	.3022	.3022
5	Piping	.1423E+01	.7170E-01	919.4330	509.00	4.4920	.3022
6	TSA	.2252E+01	.1375E+01	918.8970	509.00	1.3230	1.3230
7	Piping	.1793E+00	.7170E-01	918.8960	509.00	.3022	.3022
8	ACF	.1284E+02	.1070E+01	918.8920	509.00	1.1670	1.1570
9	Piping	.5291E+00	.7170E-01	918.8910	509.00	.3022	.3022
10	Downcomer	.1524E+01	.1340E+00	920.7370	509.00	11.3700	.4131
11	Lower Plenum	.4900E-01	.3500E-01	920.5640	509.00	.7100	.0883
12	Catch Basket	.1900E-01	.2000E-01	920.5020	509.00	.9400	.0475
13	Bypass	.2600E-01	.1160E+00	920.3090	509.00	.2200	.2967
14	Bypass	.9100E-01	.1180E+00	919.8720	509.00	.7700	.2967
15	Bypass	.9100E-01	.1065E+00	919.5960	509.00	.8200	.2675
16	Bypass	.1870E+00	.1168E+00	919.2020	509.00	1.5300	.3267
17	Bypass	.1830E+00	.1168E+00	918.5570	509.00	1.5000	.3267
18	Bypass	.1250E+00	.1114E+00	918.1280	509.00	1.0800	.2967
19	Bypass	.2400E-01	.1600E-01	917.6830	509.00	1.5000	.0258
20	Upper Plenum	.3585E+00	.1131E+00	916.6330	509.00	3.1700	.2717
21	Lower Particle Screen	.3700E-01	.4800E-01	920.4500	509.00	.7800	.2480
22	Enter T. M. Assembly	.7300E-03	.1360E-02	920.2950	509.00	.5400	.0420
23	Turbine Meter	.1050E-02	.1360E-02	920.0660	509.00	.7700	.0420
24	Enter Fuel Shroud	.7000E-03	.9000E-03	919.6600	509.00	.8200	.3000
25	Fuel	.4800E-03	.1440E-02	919.4320	509.20	.6670	.0215
26	Fuel	.9600E-03	.1440E-02	919.2510	509.40	.6670	.0215
27	Fuel	.9600E-03	.1440E-02	919.0090	509.60	.6670	.0215
28	Fuel	.9600E-03	.1440E-02	918.7670	509.90	.6670	.0215
29	Fuel	.9600E-03	.1440E-02	918.5250	510.00	.3330	.0215
30	Upper Fuel Shroud	.9200E-02	.8500E-02	916.2290	510.00	1.0800	.0833
31	Enter Instrument Housing	.2290E-01	.2760E-01	917.9050	510.00	.8300	.1880
32	Instrument Housing	.4480E-01	.6680E-01	917.7330	509.20	1.5000	.2017
33	Upper Plenum	.5870E-01	.5640E-01	915.9000	509.00	1.0400	.0542
34	Upper Plenum	.1530E-01	.2190E-01	915.5880	509.00	.7000	.0308
35	Piping	.5291E+00	.7170E-01	915.5370	509.00	.3022	.3022
36	ACE	.1284E+02	.1070E+01	915.5360	509.00	1.1670	1.1670
37	Piping	.1793E+00	.7170E-01	915.5360	509.00	1.3230	1.3230
38	TSA	.2252E+01	.1375E+01	915.5351	509.00	4.7420	.3022
39	Piping	.9019E+00	.7170E-01	913.9480	509.00	1.4170	.3022
40	Piping	.3160E+00	.7170E-01	913.9478	509.00	1.4170	.3022
41	Piping	.1029E+01	.7170E-01	913.9460	509.00	3.0000	.7500
42	Strainer	.1570E+01	.7857E+00	913.7220	509.00	.3022	.3022
43	Piping	.3140E+00	.7170E-01	913.7210	509.00	.3022	.3022
44	Piping	.5020E-01	.7170E-01	913.0990	509.00	.3022	.3022
45	Piping	.1076E+00	.7170E-01	913.0900	509.00	.3022	.3022
46	Piping	.1936E+00	.7170E-01	903.1520	509.00	7.0840	.3022
47	Piping	.6768E+00	.7170E-01	903.1510	509.00	.3022	.3022
48	Primary Bypass Piping	.7170E-01	.7170E-01	917.7630	509.00	2.0830	.3022
49	Primary Bypass Piping	.9341E+00	.7170E-01	913.4950	509.00	.4167	.3022
50	Primary Bypass Piping	.1793E+00	.7170E-01	913.1010	509.00	2.7920	.1115
51	Hx	.3645E-01	.9760E-02	912.6680	509.00	8.0830	.1115
52	Piping	.2336E+00	.9760E-02	905.9880	509.00	.1874	.1874
53	Small Hx	.5520E-01	.2760E-01	905.8690	509.00	10.6900	.1115
54	Piping	.1484E+00	.9760E-02	904.0400	509.00	.1408	.2187
55	Piping	.1776E+00	.3760E-01	903.1000	509.00	2.8340	.2187
56	Piping	.3549E+00	.3760E-01	903.1100	509.00	10.0400	.0679
57	Piping to Pressurizer	.6010E-01	.3600E-02	905.9700	509.00	2.7750	.0679
58	Piping to Pressurizer	.9990E-02	.3600E-02	905.9700	519.00	10.5000	2.2500
59	Pressurizer	.4177E+02	.3978E+01	904.0000	-1.00		

RELAP4 JUNCTION DATA USED IN ST-1 ANALYSIS

JUNCTION NUMBER	CONNECTING VOLUMES	FLOW LBM/SEC	FORWARD FLOW LOSS COEFFICIENT, KF	REVERSE FLOW LOSS COEFFICIENT, KR
1	1 to 2	26.7400	.1004E+03	.1004E+03
2	2 to 3	26.7400	.1085E+04	.1085E+04
3	3 to 4	26.7400	.2090E+01	.2090E+01
4	4 to 48	26.0090	.2500E+00	.2500E+00
5	4 to 5	.7310	.1000E-01	.1000E-01
6	5 to 6	.7310	.1000E-01	.1000E-01
7	6 to 7	.7310	.1000E-01	.1000E-01
8	7 to 8	.7310	.1000E-01	.1000E-01
9	8 to 9	.7310	.1000E-01	.1000E-01
10	9 to 10	.7310	.1000E-01	.1000E-01
11	10 to 11	.7310	.3600E+00	.3600E+00
12	11 to 12	.7310	.1050E+01	.1050E+01
13	12 to 13	.5650	.6800E+00	.6800E+00
14	13 to 14	.5850	.1420E+01	.1420E+01
15	14 to 15	.5850	.1250E+01	.1250E+01
16	15 to 16	.5850	.8200E+00	.8200E+00
17	16 to 17	.5850	.1000E-01	.1000E-01
18	17 to 18	.5850	.5900E+00	.5900E+00
19	18 to 19	.5850	.6000E+00	.6000E+00
20	19 to 20	.7285	.7400E+00	.7400E+00
21	20 to 21	.1460	.4000E-01	.4000E-01
22	21 to 22	.1460	.4500E+00	.4500E+00
23	22 to 23	.1460	0.	0.
24	23 to 24	.1460	.3100E+00	.3100E+00
25	24 to 25	.1460	.1400E+00	.1400E+00
26	25 to 26	.1460	.1000E-01	.1000E-01
27	26 to 27	.1460	.1000E-01	.1000E-01
28	27 to 28	.1460	.2000E-01	.2000E-01
29	28 to 29	.1460	.2000E-01	.2000E-01
30	29 to 30	.1460	.6900E+00	.6900E+00
31	30 to 31	.1460	.4800E+00	.4800E+00
32	31 to 32	.1460	.1240E+01	.1250E+01
33	32 to 19	.1435	.1870E+01	.1870E+01
34	32 to 20	.0025	.2100E+00	.2100E+00
35	20 to 33	.7310	.1180E+01	.1180E+01
36	33 to 34	.7310	.8300E+00	.8300E+00
37	34 to 35	.7310	.4500E+00	.4500E+00
38	35 to 36	.7310	.1000E-01	.1000E-01
39	36 to 37	.7310	.1000E-01	.1000E-01
40	37 to 38	.7310	.1000E-01	.1000E-01
41	38 to 39	.7310	.1000E-01	.1000E-01
42	39 to 40	.7310	.1000E-01	.1000E-01
43	40 to 41	.7310	.1000E-01	.1000E-01
44	41 to 42	.7310	.1000E-01	.1000E-01
45	42 to 43	.7310	.1000E-01	.1000E-01
46	43 to 44	.7310	.1000E-01	.1000E-01
47	44 to 45	25.7400	.1450E+00	.1450E+00
48	45 to 46	25.7400	.3462E+02	.3462E+02
49	46 to 47	25.7400	.3570E+01	.3570E+01
50	47 to 1	26.7400	0.	0.
51	48 to 49	26.0090	.1100E+01	.1100E+01
52	49 to 50	26.0090	.1000E-01	.1000E-01
53	50 to 44	26.0090	.1000E-01	.1000E-01
54	44 to 51	1.0000	.1000E-01	.1000E-01
55	51 to 52	1.0000	.1000E-01	.1000E-01
56	52 to 53	1.0000	.1000E-01	.1000E-01
57	53 to 54	1.0000	.1000E-01	.1000E-01
58	54 to 55	1.0000	.1000E-01	.1000E-01
59	55 to 56	1.0000	.1000E-01	.1000E-01
60	56 to 47	1.0000	.1000E-01	.1000E-01
61	55 to 57	0.0000	.6000E-01	.6000E-01
62	57 to 58	0.0000	.2500E+00	.2500E+00
63	58 to 59	0.0000	.2500E+00	.2500E+00

TABLE A-III

THE ROD AXIAL POWER PROFILE USED IN THE RIA SCOPING TEST
RELAP4 ANALYSES

Fuel Axial Location (ft.)	Normalized Power
0 to 0.333	0.211
0.333 to 1.0	0.789
1.0 to 1.667	1.0
1.667 to 2.334	0.866
2.334 to 3.0	0.490

APPENDIX B

RIA SCOPING TEST

FRAP-T4 CODE INPUT SUMMARY

APPENDIX B

FRAP-T4 INPUT PARAMETERS CORRELATIONS AND MODELING OPTIONS

The response of the RIA Scoping Test fuel rods was analyzed using the FRAP-T4 computer code. The FRAP-T4 code is a transient fuel rod thermal analysis code used to solve for the response of a fuel rod under various accident conditions. Table B-I presents a listing of the input parameters, correlations, and modeling options used in the final FRAP-T4 fuel analyses. Table B-II lists the normalized peak-to-average axial power profile, and Table B-III lists the normalized peak-to-average radial power profile used in the analyses. Table B-IV is an input summary for the FRAP-T4 analyses.

INPUT PARAMETERS, CORRELATIONS AND MODELING OPTIONS USED

IN THE FRAP-T4 CALCULATIONS FOR RIA-ST

Number of Fuel Rods = 1
Number of Flow Channels =1
Number of Axial Nodes = 18
Number of Radial Nodes = 15
Fuel Deformation Model Type = 0
Free Thermal Expansion Fuel Deformation Model Specified
Cathcart Cladding Oxidation Model Specified
Modified Ross and Stoute Model for Gap Conductance Used
Gas Flow Model Turned On
Critical Heat Flux to be Multiplied by a Factor of 1.0
Fuel Rod Length = 0.914 m
Rod Diameter = 0.00970 m
Cladding Cold Work = 0.1
Probability Threshold for Fuel Rod Failure = 1.1
Normalized Axial Variation in Fast Flux Assumed Same as that of Fuel Rod
Power
Thermal Property Data for Clad and Fuel
Geometry and Composition Specifications
Radial Power Distribution
Initial Temperature Distribution = 538.0 K (620 $^\circ$F)

Average Power History for Fuel Rod
Axial Power Profile
Enthalpy rise of coolant while flowing past fuel rods computed by RELAP4
Critical Heat Flux Option = No Cold Wall No Axial Factors
CHF Correlation = Hughes/Tong (W-3)
Post-CHF Heat Transfer Code = Groeneveld Eqn. 5.7 as Mode 5
Core Pressure History = 6.335 MPa
Equivalent Heated Diameter of rod = 0.017721 m
Equivalent Hydraulic Diameter = 0.006610 m

Coolant Flow Area = 1.338 x 10^{-4} m^2
Arithmetic Mean Roughness:
                        Cladding = 1.14 microns
                        Fuel = 2.12 microns
Initial Gas Fill Information:
                        Composition = Helium
                        Pressure = 0.103 MPa
                        Temperature = 293 K (68°F)

TABLE B-II

NORMALIZED PEAK TO AVERAGE AXIAL POWER PROFILE

Distance from Bottom of Fuel Pellet Stack (m)	Normalized Value
0.0254	0.54
0.0762	0.69
0.1270	0.85
0.1778	1.03
0.2286	1.13
0.2794	1.24
0.3302	1.30
0.3810	1.34
0.4318	1.36
0.4826	1.32
0.5334	1.28
0.5842	1.20
0.6350	1.11
0.6858	1.00
0.7366	0.87
0.7874	0.72
0.8382	0.58
0.8890	0.44

TABLE B-III

NORMALIZED PEAK TO AVERAGE RADIAL POWER PROFILE

RADIUS (m)	Normalized Value
0.000187	0.942
.000561	0.943
.000935	0.946
.001309	0.951
.001683	0.957
.002058	0.964
.002432	0.975
.002806	0.992
.003180	1.009
.003554	1.030
.003928	1.063

TABLE B-IV

FRAP-T CODE INPUT SUMMARY

		9.70-mm OD Fuel Rod	10.7-mm OD Fuel Rod
Fuel Region	Active Length (m)	0.9144	0.9144
	Material	UO_2	UO_2
	Enrichment (%)	5.7	20
	Pellet Height (mm)	15.2	15.49
	Pellet Diameter (mm)	8.24	9.3
	Pellet Shoulder Radius (mm)	3.3	3.1
	Dish Depth (mm)	0.343	0.33
	Density (kg/m^3)	10083	10276
	Theoretic Density (%)	94.5	93
	RMS Roughness	2.12	2.12
Cladding Region	Material	Zircaloy 4	Zr. 4
	Cladding ID (mm)	8.42	9.51
	Cladding OD (mm)	9.70	10.73
	RMS Roughnes	1.14	1.14
Plenum Region	Gas Quantity (moles of He)	0.000282	0.0103
	Plenum Volume (mm^3)	2290	6720
	Gas Pressure (MPa)	0.1034	2.6
	Spring Length (mm)	50.8	50.8
	Spring Coil OD (mm)	8.23	9.02
	Spring Wire Diameter (mm)	1.02	1.02
	Number of Spring Coils	17	17
Flow Shroud	Coolant Flow Area (mm^2)	133.8	118.5
	Hydraulic Diameter (mm)	6.61	5.58
	Equivalent Heated Diameter (mm)	17.72	14.1